NANYANG TECHNOLOGICAL UNIVERSITY

STATIC AND DYNAMIC VOLTAGE STABILITY ANALYSIS

STATIC AND DYNAMIC VOLTAGE STABILITY ANALYSIS

POTHULA UMA MAHESWARA RAO

POTHULA UMA MAHESWARA RAO

SCHOOL OF ELECTRICAL & ELECTRONICS ENGINEERING

2007

2007

Static and Dynamic Voltage Stability Analysis

Pothula Uma Maheswara Rao

School of Electrical & Electronics Engineering

A thesis submitted to the Nanyang Technological University
in fulfilment of the requirement for the degree of
Master of Engineering

2007

Abstract

Voltage instability has been a great concern for quite a long time in electric power industry. A system enters a state of voltage instability due to increase in demand, a sudden large disturbance or a change in system condition that causes a progressive and uncontrollable decline in voltage. It is therefore interest to study both the dynamic and static aspects of voltage stability. Dynamic voltage stability can be divided into short-term and long-term based on the dynamics of the components that affect the voltage stability.

In this study, dynamic models of various power system components (such as on load tap changing (OLTC) transformers, over excitation limiters (OXL), generators, induction motors, exponential loads etc.,) are successfully developed in MATLAB/ SIMULINK platform. The effect of induction motor load on short-term voltage stability of a simple power system is investigated using the network and motor *P-V* curves and the results found are then verified by observing the system states in time domain. The effects of the dynamics of slow-active devices, such as OLTC of a transformer, OXL of a generator, etc., on long-term voltage stability of a power system are also investigated in time domain. A computer program in MATLAB / SIMULINK environment is developed to investigate the long-term voltage instability and identify the reasons for dynamic voltage instability. Once the reason of voltage instability is identified, a remedial action using fixed capacitive reactive support is suggested to prevent the voltage instability. During a fault, the system voltage reduces drastically and that may cause to stall the induction motors. Stalling of induction motor can be prevented by clearing the fault as quickly as possible. A technique of determining the critical fault clearing time to prevent stalling of induction motor is also presented.

In power system operation, it is important for the dispatcher to have knowledge on the maximum permissible loading of the system without reaching voltage instability. In this study, a method of determining the voltage stability index of a system based on the complex voltage of all buses in the system is described. The proposed index is then used in estimating the maximum loading of the system and is based on the information of present and past operating points. In addition, the weakest segments

(critical bus and critical line) of the system are also identified for appropriate reactive compensations to avoid voltage collapse. The correctness of the identified critical bus and critical line is then verified by placing shunt/series capacitors at various locations and comparing the corresponding critical load multiplier factors.

Acknowledgements

I would like to express my sincere appreciation and gratitude to my supervisor, Associate professor Mohammed Hamidul Haque, for his invaluable guidance and consistent encouragement throughout the course of this work. His advice and assistance in the preparation of this thesis is thankfully acknowledged.

Acknowledgement is extended to Professor Choi San Shing, former head of the division of power engineering, for the opportunity given to pursue a research degree. Truly appreciated is the financial support granted by the Nanyang Technological University as postgraduate research scholarship.

I would also like to thank my colleagues and laboratory staff at the division of power engineering for interesting discussions and providing a pleasant working atmosphere. Thanks also to many other friends and relatives for their support and encouragement and for making my stay in Singapore more enjoyable.

Finally, I would like to thank my family members, in particular my mother and my father who have been a constant source of inspiration throughout my academic career.

Table of Contents

List of Figures page

List of Tables page

List of Abbreviations

OLTC	On Load Tap Changers
OXL	Over Excitation Limiters
FACTS	Flexible AC Transmission Systems
SVC	Static Var Compensators
ULTC	Under Load Tap Changers
TCUL	Tap Changers Under Load
LTC	Load Tap Changer
AVR	Automatic Voltage Regulator
PoC	Point of Collapse
GPS	Global Positioning Systems
PMU	Phasor Measuring Units
VSI	Voltage Stability Index
LVSI	Line Voltage Stability Index
PVSI	Path Voltage Stability Index
LHS	Left Hand Side

Glossary

Variables

Generator

V_g	generator terminal voltage
I_g	generator terminal current
i_d	direct axis winding current component
i_q	quadrature axis winding current component
E_q	quadrature axis open circuit voltage
E'_q	emf behind transient reactance
H	inertia coefficient
P_m	mechanical power produced by the turbine.
S_g	electrical power produced by the generator
δ	generator rotor angle
ω	generator rotor speed
D	damping coefficient
T'_{do}	open circuit transient time constant
X_d	direct axis synchronous reactance
X_q	quadrature axis synchronous reactance
X'_d	direct axis transient reactance
v_{fd}	generator excitation voltage
$v_{fd}^{\max}$	generator maximum excitation voltage
$v_{fd}^{\min}$	generator minimum excitation voltage
V_{ref}	generator AVR reference voltage
G	AVR regulator gain
T	AVR regulator time constant
I_{fd}	generator excitation current
$I_{fd}^{\lim}$	generator excitation current limit
S_1, S_2	OXL slope constants
K_1, K_2, K_r, K_i	OXL constants

x_{oxl}	OXL output

OLTC

V_{ref}	reference voltage
ΔV	voltage difference
D	dead band
ε	directional tolarence sensitivity
T_d (T_{d0} ,T_{d1})	time delay for time delay element
T_m	time constant for the motor drive unit
e	output of measuring element
b	output of time delay element
Δn	output of motor drive unit
n_i	next step tap position
$n_{(i-1)}$	current tap position
Δu	per unit voltage change
t_r	tap ratio

Induction Motor Load

T_e	Motor electrical torque
T_m	Motor mechanical torque
T_c,	coefficient of the constant component of load torque
T_s	coefficient of the static component of load torque
T_q	coefficient of the quadratic component of load torque
ω_m	rotor speed
H	inertia coefficient
s	slip
s_0	pre-fault stable slip,
t_{cr}	critical fault clearance time
R_r	rotor resistance
X_r	rotor reactance
X_m	motor magnetic reactance
X_s	motor stator reactance

R_s	stator resistance
V'_{th}	thevinin equivalent voltage
$\boldsymbol{V_c}$	complex voltage across rotor terminals
$\boldsymbol{V_t}$	complex voltage at motor terminals
I_s	stator current
P_{ag}	air-gap power
I_r	rotor current
V_r	voltage across resistance R_r/s

Exponential Load

a , b	exponent values
V_0	reference voltage
P_0, Q_0	real and reactive powers at reference voltage
P_{ss} , Q_{sl}	real and reactive powers drawn by exponential load

P-V curve

V_s	stable voltage
V_u	unstable voltage
P_{cr}	critical power
s_{cr}	critical slip
V_{cr}	critical voltage

Multi Bus System

V_l , I_l	load voltage and current
$E_{th}\angle\theta_{th}$	thevenin equivalent source
X_{th}	thevenin reactance
Y (=G+jB)	admittance matrix of the system.
P_{Li}, Q_{Li}	active and reactive components of load (sum of static and induction motor load) at bus i.
V_i, θ_i	voltage magnitude and phase angle at bus i
P_{gi}, Q_{gi}	active and reactive components of the generator power at bus i

$\mathbf{Z}_{ij}$, $\mathbf{Z}_{ij1}$ and $\mathbf{Z}_{ij2}$	equivalent mutual impedance, shunt impedance on side '*i*' and side '*j*' respectively
a	off-nominal turns ratio of the transformer
ζ	a set of lines in the critical power flow path
λ	load-multiplying factor
λ_{cr}	critical load multiplier factor

Chapter 1

Introduction

1.1 Background, Motivation and Objective

1.1.1 Background

Deregulation of power industry has brought major changes in power transmission requirements. These challenges come together with a growing intolerance to poor power quality introduced by increasingly sophisticated manufacturing and service industries, and the society as a whole, which cannot tolerate power outages and other disturbances affecting their operation. The potential problems are further aggregated by social, environmental, right of way cost, which hinder the construction of new transmission lines. Introduction of the deregulated energy market has lead to severe stressing of the transmission grid due to the operation of the grid to its maximum financial returns with limited investment in it. One of the major problems that is associated with a stressed system is voltage instability or voltage collapse. *Voltage Collapse* is a process, which leads to reduction of voltage in a significant part of a power system [1-5]. The tripping of transmission or generation equipments often triggers voltage collapse. In recent years, voltage collapse has become one of the major reasons for system blackouts. In 2003, five blackouts occurred within six weeks and affecting 112 million people in the US, UK, Denmark, Sweden and Italy [6-7].

There are two different approaches to analyze the voltage collapse problem, static and dynamic. Static methods involve the static model of the power system components and these methods are especially important in the case of power system operation and planning stages to make an adequate plan for meeting the power requirements during different types of contingencies. The dynamic methods use time domain simulations to reveal the voltage collapse mechanism, i.e. why and how the voltage collapse occurs. Dynamic methods analyze the effect of dynamic loads, on load tap changers (OLTC), generator over excitation limiters (OXL), etc on the voltage collapse.

Power system operation mainly depends on the interaction of three things such as power sources, loads and network [1-5]. There are some events, which can induce voltage collapse viz loss of a generating unit, a transmission line, or a transformer during a load pick up. Sometimes if the setting of the tap position of an OLTC is too low, it may create reverse action instead of helping the system. In case of generators,

if the excitation hits its limit then it will create a considerable impact on the voltage stability.

During the past twenty years, there has been a continually increasing interest and investigation on voltage instability and collapse. The first paper related to voltage instability had appeared in 1968 [8]. In 1975, Venikov et al., [9] proposed the first criteria for detecting the point of voltage collapse. Even though voltage instability has been known for a long time, active work involving voltage stability started in 1980's.

The system stability mainly depends on the performance of its components for a sudden disturbance. In power systems, some of the components which are mainly responsible for the system instability are non linear in nature e.g. generators, motors, load devices, tap changers (controllers), etc. System stability mainly depends on the interaction between the devices connected to it. So it is necessary to model all the components individually in order to have proper idea about their performance. Voltage can be controlled in three ways i.e., by adjusting the generator excitation, by using OLTC or by providing reactive power support.

Voltage stability or voltage collapse deals with the ability of a power system to maintain acceptable voltage levels at all buses in the system both under normal condition and after being subjected to a disturbance. A heavily loaded system enters a state of voltage instability due to a sudden large disturbance or a change in system condition that causes a progressive and uncontrollable decline in voltage. The main factor causing voltage instability is the inability of the power system to meet the demand for reactive power.

1.1.2 Motivation

In the new electricity markets, dynamic performance and stability are becoming a major concern in the design and operation of many power systems due to the increased power transfers. It is therefore particular interest to study the dynamic stability aspect of the system besides the steady state stability aspect.

For voltage stability study, many software have been developed for both research and commercial purposes. Description of some of the software is given in [10]. For example, *UWFLOW* developed by University of Waterloo, Canada, *ASTRE* developed by University of Liege, Belgium, *CPF/EQTP* from Iowa State University, USA, *AVS* from University of New South Wales, Australia, *VOSTA* from Polytechnic of Milan and University of Pavia, Italy, *VSA* from Siemens, USA, *VSAT* from Powertech labs Inc, Canada, *EUROSTAG* from Tractebel Engineering, Belgium, *ETMSP* from *EPRI*, USA, *NETOMAC* from Siemens.

Some of the efficient professional software for dynamic analysis are very expensive and those with embedded models sometime lack in transparency. Modification of these software for research purpose is difficult and also takes time to become master on the complex software. MATLAB is widely used in universities, and SIMULINK is the well-known environment for dynamic system simulation and development [11].

The purpose of this research is to investigate the effect of various components of a power system such as OLTC, OXL etc, on the dynamic voltage stability of the system. Also one of the root causes for voltage stability problem is the reactive power deficit in the system particularly near load centers. It is important to alleviate the voltage stability problem by providing reactive power support to areas that are critical in terms of reactive power. Several methods are reported in the literature to determine voltage stability margin/index based on the system Jacobian. Jacobian based methods utilize either sensitivity or eigenvalue behavior of the Jacobian matrix to determine the closeness to singularity. These methods are computational intensive and time consuming [3]. However, some methods reported in the literature suggest that the local voltage and current phasors contain information to identify the areas, which are prone to voltage collapse [12]. The idea of using voltage and current phasors information to determine the steady state voltage stability index of a general power system has inculcated enough motivation to develop an algorithm, which can identify areas prone to voltage collapse, and to suggest a method to alleviate it.

1.1.3 Objectives

Voltage stability of a power system in real time depends on the interaction between various components such as OLTC, OXL, AVR, generators, induction motors, etc. The objectives of this research are:

- To study and implement various standard components of power system using MATLAB/SIMULINK software.
- To investigate the influence of disturbances on short-term voltage stability in a simple power system with induction motor load
- To investigate the influence of disturbances on long-term voltage stability in a simple power system with OLTC transformer, generator OXL and composite load
- To investigate the static voltage stability of a general power system and identify its critical bus and line based on the complex bus voltages

1.2 Contributions of the Thesis

The main contributions of the thesis are summarized as follows

- Standard mathematical models of various power system components, such as induction motor, OLTC, and generator with OXL and AVR have been studied. The studied models are then implemented using MATLAB/ SIMULINK software.
- The implemented MATLAB/SIMULINK models of various power system components have been integrated to investigate the effect of disturbances on dynamic voltage stability of a power system.
- The critical fault clearing time of a radial system to avoid stalling of an induction motor due to voltage reduction has been determined.
- A method of investigating the static voltage stability of a general power system and to identify the critical bus and critical line, using the information of complex bus voltages has been developed.

1.3 Organization of the Thesis

The thesis is organized as follows

Chapter 1 describes the background, motivation, objectives and contributions of the research work.

Chapter 2 presents the literature review on the static and dynamic voltage stability of a power system.

Chapter 3 identifies the reasons for dynamic voltage instability and described some standard mathematical models of various power system components. These components are then implemented in MATLAB/ SIMULINK software. The MATLAB/ SIMULINK models are then used to investigate the effects of various components (induction motor, transformer with OLTC, and generators with OXL and AVR) on dynamic stability of a simple system due to sudden disturbances. A method of determining the critical fault clearing time of a radial system to avoid stalling of induction motor load is also proposed. Based on the investigations, a remedial action to prevent the voltage collapse is also explored and presented.

Chapter 4 presents a method of determining the static voltage stability index of a general power system. First an expression for line voltage stability index (*LVSI*) of a simple two-bus system is derived. The concept of the *LVSI* is then extended for a general power system to identify the critical power flow path that initiates voltage instability. Based on the value of *LVSI* of each line of the critical path, the critical line as well as critical bus of the system is identified. The effectiveness of the above concepts is then tested on the IEEE 30 bus system and the results found are compared with the corresponding actual values.

Chapter 5 ends the thesis with conclusions and recommendations.

Chapter 2

Literature Review

2.1 Introduction

Voltage stability or voltage collapse has become a major concern in many modern power systems. In the deregulated market conditions, a power system is set to operate at its maximum operating limits for better utilization of existing facilities. Such a system cannot withstand for any network outage and thus it is important to study the system behavior in the case of prolonged overload and/or any system disturbances.

Formal definitions of the terms related to voltage stability are given in [13, 14]. *Voltage Stability* is the ability of a power system to maintain voltage irrespective of the increase in load admittance and load power resulting in control of power and voltage. The process by which voltage instability leads to loss of voltage in a significant part of a power system is called *Voltage Collapse*. The ability of a power system to operate not only in stable condition but also to remain stable following any reasonable contingency or adverse system change is termed as *Voltage Security*.

A system enters into the unstable state when a disturbance (load increase, line outage or other system changes) causes voltage drop quickly or drift downward, and automatic system controls fail to improve the voltage level. The voltage decay may take a few seconds to several minutes.

2.2 Classification of Power System Stability

Power system stability is classified as rotor angle stability and voltage stability [1, 2, 3, 10, 13, 14]. Table 2.1 shows the power system stability classification based on time scales and driving forces. Time scales are divided into short-term (few seconds) and long-term (few minutes). Based on the instability driving forces, stability is classified as load driven or generator driven.

The rotor angle stability is divided into small-signal and transient stability. The small-signal stability deals with small disturbances in the form of undamped electromechanical oscillations. The transient stability is due to lack of synchronizing torque and is initiated by large disturbances. The time frame of angle stability is that of the electromechanical dynamics of the power system. This time frame is called

short-term time scale, because the dynamics typically last for a few seconds. Time scale of short-term voltage stability and rotor angle stability is the same and sometimes it is difficult to differentiate between short-term voltage stability and rotor angle stability. In the long-term time scale where the short-term dynamics have already died out, two types of stability problems emerge based on frequency and voltage. Frequency instability related to the active power imbalance between generators and loads [1-3]. The long-term voltage stability is characterized by the actions of the devices such as delayed corrective actions and load shedding [1-3].

Table 2.1 Power system stability classification

<table>
<tr><td>Time scale</td><td colspan="2">Generator-driven</td><td colspan="2">Load-driven</td></tr>
<tr><td rowspan="2">Short-term (few seconds)</td><td colspan="2">Rotor angle stability</td><td colspan="2" rowspan="2">Short-term voltage stability</td></tr>
<tr><td>Transient</td><td>Small signal</td></tr>
<tr><td rowspan="2">Long-term (few minutes)</td><td colspan="2" rowspan="2">Frequency stability</td><td colspan="2">Long-term voltage stability</td></tr>
<tr><td>Small disturbance</td><td>Large disturbance</td></tr>
</table>

Table 2.2 Power system component and load classifications

Time scale	System component	Type of load
Instantaneous	Network	Static loads
Short-term	Generators, Switching capacitors/reactors, FACTS, SVC,	Induction motors
Long-term	OLTC, OXL	Thermostatically controlled loads

Voltage stability is also called as load stability because of the nature of the stability and it is driven by the load dynamics. It can be divided into instantaneous, short-term and long-term voltage stability according to the time scale of load dynamics. System components that affect the instantaneous, short-term and long-term stability are given in Table 2.2. Network and static loads are classified as instantaneous components of the system because of their instantaneous response to changes in the system. Short-

term voltage stability depends on the performance of the various components like excitation of synchronous generator, induction motor, switching capacitors and electronically controlled devices such as static var compensators (SVC) and flexible AC transmission systems (FACTS). Long-term voltage stability depends on the slow responding components like OLTC, OXL, thermostatic loads, etc. [1-3]

For the purposes of analysis, it is sometimes useful to classify the voltage stability into small and large disturbances. Small disturbance voltage stability considers the power system's ability to control voltages after small disturbances, e.g. changes in load [1-3]. The small disturbance voltage stability is investigated through steady state analysis. In such a case, the power system can be linearised around an operating point and the analysis is typically based on eigenvalue and eigenvector techniques. Large disturbance voltage stability investigates the response of the power system to large disturbances e.g. faults, switching or sudden loss of load or sudden loss of generation, etc [1-3]. Large disturbance voltage stability can be studied by using non-linear time domain simulations in the short-term time frame, whereas in long-term time frame load flow analysis along with non-linear time domain simulations are used [1-3]. The voltage stability is, however, a single problem in which combinations of both linear and non-linear tools are to be used.

Historically power system stability has been considered based on synchronous operation of the system. However, many power system blackouts all over the world have been reported where one of the reasons for the blackout has been identified as voltage collapse.

2.3 Some of the Power System Voltage Collapses and Blackouts

During the year 2003, a number of blackouts occurred over a span of less than two months affecting millions of people around the world. Some of them are:

Cascading failure of transmission and generation outages, which caused worst ever blackouts in the history of Northeast United states and Canada, on 14 August. Blackout left more than 50 million people in the dark [6, 7].

Line faults followed by line tripping and malfunctioning of protection relays caused a blackout affecting 5 million people in Sweden and Denmark on 23 September. A similar blackout happened in Italy on 28 September, which has left 57 million people in the dark. This is one of the worst blackouts in Europe [6, 7].

Another blackout, which is different from the United States and Europe, occurred in United Kingdom on 28 August due to transformer outage and a faulty relay operation [6, 7].

Some of the blackouts that took place in the last decade are as follows:

A short circuit on a transmission line initiated a chain of events leading to a break-up of the Western North American power system on 2 July 1996. The reasons for the break-up were rapid overload, voltage collapse and angular instability [6].

Tripping of a generating unit, transmission line and a manual reduction of reactive power in another generating unit caused an initial decline in voltage and thereby leading the system to blackout in Finland on 10 August 1992. Similarly, tripping of four thermal units which resulted in the tripping of nine other thermal units followed by eight other units because of the over excitation field current protection defects caused blackout in France on 12 January 1987 [1].

A brush fire caused tripping of three lightly loaded transmission lines thereby resulting in voltage collapse and blackout within a few seconds in South Florida on 17 May 1985 [1].

A disconnector failure and fault at a substation in Stockholm resulted in loss of the substation and two transmission lines. Followed by cascading of line outages and tripping of nuclear power units due to excess current protection led Sweden into isolation and total blackout on 27 December 1983 [1].

A heavy system loading causing low voltage profile and exhaustion of the reactive power resources resulted in voltage collapse in France on 19 December 1978 [1].

2.4 Influence of Different Power System Components on Dynamic Voltage Stability

From the above mentioned blackouts along with the respective causes for blackouts, it is clear that the slower acting devices such as on load tap changers, generator over excitation limiters, characteristics of the system loads and also fast acting devices such as induction motors, excitation system of synchronous machines and compensation devices contribute to the evolution of voltage collapse due to sudden disturbances in the power system [1-3].

Tap changers are the devices in main power delivery transformers, which are the main mechanisms operating in regulating the voltage automatically. Tap changers control the voltage by changing the transformer turns ratio. In many cases, the variable taps are on the high voltage side because of the lower current and easier commutation. Various acronyms have been suggested for the transformer tap changer mechanisms: on load tap changers (OLTC), under load tap changers (ULTC), tap changers under Load (TCUL), and load tap changers (LTC) [1-3].

Two types of tap changer models are commonly used i.e., continuous and discrete types. Continuous models are based on the assumption of continuously changing taps whereas discrete models are based on the discontinuous or step-by-step tap change. In the present work discrete type OLTC have been considered [3]. Typically a transformer equipped with an OLTC feeds the distribution network and maintains constant secondary voltage. OLTC operates with a certain delay depending on the difference between the reference and actual voltages at OLTC input.

The effect of reverse action of a tap changer, more precisely, the phenomenon of raising the position of on-load tap changer for raising the secondary voltage causes the drop of secondary voltage [15-16]. The secondary voltage of a transformer is usually maintained at a level higher than its lower bound by the automatic OLTC even

if the voltage of primary transmission system drops. However, if the load demand becomes excessive, the secondary voltage becomes unstable. The instability of the tap changer is caused by the fact that the tap changer tries to keep the secondary voltage constant that results in maintaining the load demand constant, in worse cases, increasing it. The reverse action caused by the tap changer could occur when the initial operating voltage in the secondary side of the transformer is far less than the rated value. The effect of OLTC transformer and SVC on steady state voltage stability has been studied in [17]. The effects of OLTC transformers on voltage stability and the identification of the critical OLTC transformers out of the available OLTC transformers in a general power system have been studied in [18].

Synchronous generators are the primary devices for voltage and reactive power control in power systems. According to power system security, the most important reactive power reserves are located there. In voltage stability studies, active and reactive power delivering capabilities of generators are needed to achieve the best results. High reactive power demand by the loads may cause the generators to lose their ability to act as a constant voltage source because of the field current limits. For such a case the generator behaves like a voltage source behind the synchronous reactance and its terminal voltage reduces. While studying the voltage stability/voltage collapse phenomena, the effects of the excitation system and the automatic regulators are often simplified and/or neglected. The researchers are now paying attention to the excitation system. K. Walve [19] first suggested the effect of excitation system limits on voltage stability in 1986. If the generator hits the reactive power limits, the power system may become unstable due to lack of reactive resources. There are two causes of the reactive power output of a generator reaching a limit; excitation current limit (over excitation and under excitation) and the stator current limit. Stator current limiter is commonly used to limit reactive power output to avoid stator overloading. The action of the stator current limit is disadvantageous for voltage stability [20]. The stator current limiter decreases the reactive power capability to avoid stator over heating and causes dramatic decrement in voltage. An approach that focused on the excitation/automatic voltage regulator (AVR) system limits was presented in [21]. It is important for voltage stability to have enough buses in a power system where voltage may be kept constant. The AVR of synchronous generators are the most important for that. The action of modern AVR's is fast

enough to keep voltage constant. Steady state studies have related reactive power generation limitations to the sudden onset of voltage instability. The relationship between the dynamic models and steady state behavior is established in [22]. The dynamic performances of a power system with generators operating under rotor current limitation and over excitation limiters have been analyzed in [23]. In some cases, it is shown that in certain cases the field current limitation introduces slow generator dynamics that interact with the long-term dynamic devices, such as OLTCs, whereas in other cases the generator dynamics remain fast even after the limitation of rotor current.

Loads are the driving force of voltage instability, and that is why the voltage instability has also been called as load instability. Exact modeling of loads is a difficult problem because in the power system loads are aggregation of many different devices. The heart of the problem is the identification of the load composition at a given time and the modeling the aggregate. The nature of the differential equations for induction motors, tap changing near static load and heating system are highly nonlinear and very difficult to parameterize for model estimation [24-26]. A somewhat simpler, but still nonlinear model was proposed based on the assumption of exponential recovery. The first-order variable admittance model and the aggregate nonlinear recovery model have been considered along with the system dynamic equations to obtain the dynamic voltage stability limit of a power system [27]. The adequacy of these two models has been verified with third order induction motor model for the representation of induction motor loads.

A short circuit in a network reduces the voltage, which in turn reduces the electrical torque developed by an induction motor and that cause to decelerate the motor. The speed reduction or slip increase of induction motor depends on the mechanical torque demand and motor inertia. During the short circuit, induction motors absorb a greater amount of reactive power and operate at low power factors which may further decrease the voltage and may finally result in the stalling of the motors [28, 29].

From the viewpoint of dynamic phenomena, the voltage collapse starts locally at the weakest bus and spreads out to the other weak buses. Cascaded voltage collapse was analyzed with dynamic simulation of induction motor models in [30].

2.5 Various Voltage Stability Analysis Methods

Voltage stability stems from the attempt of load dynamics to restore power consumption beyond the capability of the combined transmission and generation systems. The controllers have their own physical limits. In general, under normal situation voltage can be maintained within the limits. But when major outages or large demand occur, the controllers may reach their limits. With the increased loading and exploitation of the power transmission systems, the problem of voltage stability attracts more and more attention. A voltage collapse can take place in systems and subsystems, and can appear quite abruptly. Continuous monitoring of the system state is therefore required. A voltage collapse occurs because of the insufficient reactive power support at the weak buses. The voltage instability problem can be alleviated by providing additional reactive power support through fixed or switched capacitors [31].

A voltage collapse proximity indicator of load buses of a power system based on optimal impedance solution has been proposed and investigated in [32]. The performance of the indicator was investigated for two types of load increment, i.e., the load increase at a particular bus and the load increases throughout the system. The indicator is capable of providing a good indication about the maximum possible power that could be delivered to the load when there is a single load variation in the system. However, when the load in the entire system is increased the indicator could predict the maximum possible power less accurately than the single load variation.

Reference [33] described a method that can identify the regions experiencing voltage collapse and the equipment outages that cause voltage collapse in each of these regions. This method identifies whether the voltage collapse caused by a contingency is due to clogging voltage instability (occurs due to increased transfer, wheeling or load pattern) or loss of control voltage instability (occurs due to equipment outages). The advantage of this method is that it requires little computation and is comprehensive in attempting to find all regions with voltage collapse problems and all single and double equipment outages that cause voltage collapse in each region. The implementation of both point of collapse (*PoC*) and continuation methods for the computation of voltage collapse points in large *AC/DC* systems were also presented in [34]. An algorithm for identifying the strategic location for compensation devices has

been proposed in [35]. Several other methods, such as model analysis using snap shots, test function, bifurcation theory, energy function methods, bus participation method, singular value method, optimization techniques, quasi steady-state method, multi time scale method, binary search method, sensitivity analysis and load flow index method have been reported in the literature [3, 10, 36-38].

Tracking stability margins has always been a demanding problem because of nonlinearity. A method (SMARTDevice) to estimate the proximity of voltage collapse using the local measurements (bus voltages and load currents) has been proposed in [39]. This method determines the relative strength/weakness of the transmission system connected to a particular load bus. Based on local measurements it produces an estimation of the strength/weakness of the transmission system connected to the bus, and compares that with the local demand. The closer the local demand is to the estimated transmission capacity, the more imminent is the voltage instability. SMART Device (stability monitoring and reference tuning device) operates on the principle that at voltage collapse point the magnitude of the Thevenin impedance (Thevenin equivalent of the network as seen from the local substation) is equal to the magnitude of the load apparent impedance. In this method Thevenin equivalent impedance is obtained from some locally measured data [39, 40].

To operate the system with in an adequate security margin, it is important to estimate the maximum permissible loading of the system. *P-V* and *Q-V* curves are very commonly used to determine the maximum permissible load (static voltage stability limit) of a power system. Bonneville power administration uses the conventional *P-V* and *Q-V* curves as a tool for assessing the voltage stability of the system [41]. However *P-V* and *Q-V* curves are highly nonlinear around the maximum permissible power point. The gradient of the curves changes sign at maximum permissible power point. Thus estimation of critical load using information at a particular operating point may not provide the correct result without practically generating the entire curves. A simple method based on *V-I* characteristic has been proposed to estimate the critical load at the verge of voltage collapse [42]. This method requires bus voltage and current data at present and some past operating points. The bus voltage and current data required for preparing the *V-I* characteristic are readily available in all power system. The voltage and current data are processed through the least squares method

to generate the *V-I* characteristic. The extrapolated part of the characteristic is then used to estimate the critical load at the verge of voltage collapse. The advantage of this method is that it does not require the knowledge on other system parameters or system wide information.

A stability factor method to identify the critical lines instead of critical buses of a power system was proposed in [43]. The stability factor method was then compared with three established methods. The first method is the Lee's method of stability margins that uses stability margin as voltage stability criterion for determining whether the system is stable. The bus that has a stability margin closer to zero is considered as critical bus [44]. Second method is the Kessel's stability indices method, which computes the stability index of each bus in the system and identifies the bus with high index values as critical ones [45]. The third method is the Schlueter's stability indicators method developed based on the changes in the load flow Jacobian. The stability indicator that is a measure of the proximity to voltage collapse is then determined from the eigenvalues of the load flow Jacobian. The eigenvalues are estimated for all load buses. The buses in a secure voltage control area should have larger eigenvalue. The eigenvalue for the critical bus decreases to less than unity and that could be the origin of voltage collapse [33].

In the recent years, it is possible to synchronize the sampling process in distant substations economically by using the global positioning systems (*GPS*). Phasor measuring units (*PMUs*) (the basic hardware box that converts current and voltage signals into complex phasors) using synchronization signals from the *GPS* satellite systems have evolved into mature tool now [46].

When a major disturbance occurs, protection and control systems have to limit the impact, stop the degradation and restore the system to a normal state by appropriate corrective actions. Wide area measurement and protection systems limit severity of disturbances by early recognition as well as proposition and execution of coordinated stabilizing actions. A system design based on the synchronized phasor measurement units, encouraging system protection schemes for frequency, angle and voltage instabilities has been proposed in [47, 48].

The location of the critical node and the critical transmission path cannot be identified in a simple way. Some of the methods determined the critical node by checking the system's closeness to singularity through either sensitivity or eigenvalue behavior of the system's Jacobian matrix. This causes a computational burden for real-time voltage stability estimation. However, Voltage phasors contain enough information to detect the voltage stability margin of a power system. Based on the voltage phasors approach, a voltage collapse proximity index for identifying critical transmission paths with respect to the real or reactive power loading has been proposed in [12]. In this method, the difference between the halved voltage phasor magnitude of relevant generator and the voltage drop along the transmission path is considered as transmission path stability index. Two types of transmission paths i.e. active transmission path (a sequence of connected buses with declining phase angles starting from a generator bus) and reactive power transmission path (a sequence of connected buses with declining voltage magnitudes again starting from a generator bus) were proposed. In this method, if the value of transmission path stability index reaches zero, the power transfer on that transmission path becomes unstable due to voltage collapse.

Chapter 3

Evaluation of Dynamic Voltage Stability

3.1 Introduction

Voltage stability or voltage collapse is an important issue in the deregulated electric power system operation. It can be classified into short-term and long-term based on time scale of operation. In short-term, the dynamics of fast acting devices, such as generators, induction motors, switched capacitors, etc. determines the system performance. However, in long-term the dynamics of slow acting devices, such as over excitation limiters (OXL) of generators and on load tap changers (OLTC) on the transformers, etc., comes into effect [1-3].

This chapter mainly focuses on the short-term and long-term dynamics of various power system components in radial and mesh networks. When a severe disturbance, such as fault, line tripping, etc., occurs, the voltage of some buses reduces drastically. Reduction of system voltage may cause to stall the heavily loaded induction motors and that may ultimately lead to voltage instability.

The voltage instability initiated by an induction motor load belongs to the category of short-term stability. Analysis of such stability requires the results in time domain to understand the mechanism or reason of voltage collapse. System states in time domain also provide the information on the chronology of voltage instability process following a large disturbance [3].

Induction motor load is an important component of the system load, which contributes to voltage instability. However, it is a fast restoring load (in the time frame of seconds) and requires high reactive power. Also it is prone to stalling when the system voltage decreases to a certain level, especially at higher mechanical load, for a longer duration. The voltage at the supply terminals of the motor should be restored before the motor slip reaches an unacceptable value.

In order to investigate the long-term voltage stability, OXL on local generators and OLTC on the transformers are considered. Also a technique of improving the voltage stability performance of the system is suggested and investigated.

3.2 Short-Term Voltage Stability

This section investigates the phenomenon of short-term voltage stability of a simple power system caused by a heavily loaded induction motor load. The mechanism of voltage collapse (i.e. why and how it occurs) is also identified.

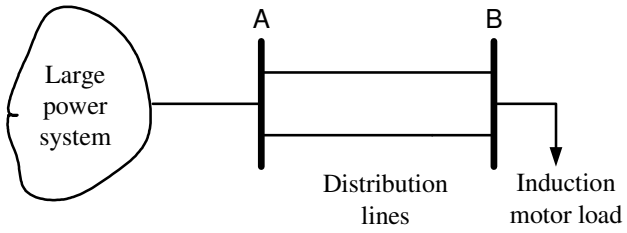

Fig. 3.1 Single line diagram of study system for short-term voltage stability

3.2.1 Study System and its Mathematical Model

In the study system, it is considered that a load bus 'B' is supplied by a large power system through a double circuit distribution lines as shown in Fig. 3.1. The load may consist of a large number of induction motors. However, in voltage stability studies, these motors are usually aggregated and represented by a single equivalent induction motor. The overall equivalent circuit of the system is shown in Fig. 3.2.

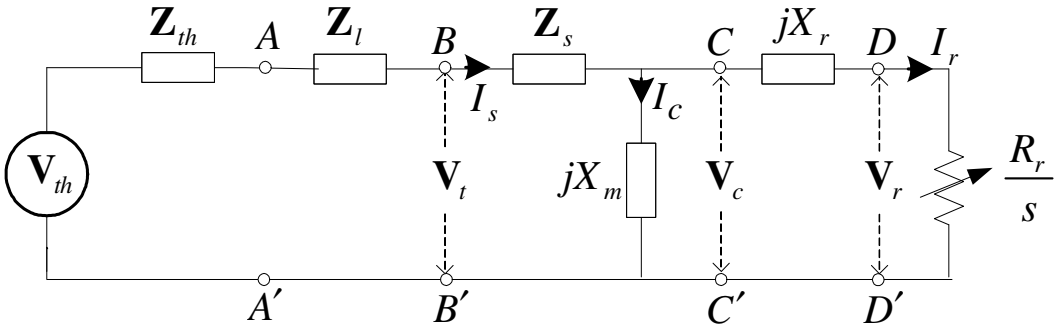

Fig. 3.2 Equivalent circuit diagram of the study system shown in Fig. 3.1

The power system feeding bus 'A' is represented by its Thevenin equivalent circuit consisting of a fixed Thevenin voltage source ($\mathbf{V}_{th}$) in series with Thevenin impedance

($\mathbf{Z}_{th}$). Distribution lines are represented by series impedance ($\mathbf{Z}_l$). The circuit to the right of BB' represents the equivalent circuit of the aggregated induction motor load [1-3]. $\mathbf{Z}_s$, X_m, X_r, and R_r are the impedance of the stator winding, the magnetizing reactance, rotor reactance and rotor resistance of the induction motor respectively. I_r and V_r are the current through and voltage across the rotor resistance R_r/s, where s is the operating slip of the motor.

Voltage across the rotor terminals (at the point CC') in the Figure 3.2 can be expressed as

$$\mathbf{V}_c = \mathbf{V}_r + j\mathbf{I}_r X_r \tag{3.1}$$

The motor terminal voltage $\boldsymbol{V}_t$ (at points BB' of Fig. 3.2) can be written as follows

$$\mathbf{V}_t = \mathbf{V}_c + \mathbf{I}_s \mathbf{Z}_s \tag{3.2}$$

where $\mathbf{I}_s = \mathbf{I}_r + \mathbf{I}_c$ and $\mathbf{I}_c = \dfrac{\mathbf{V}_c}{jX_m}$

In terms of terminal voltage ($\boldsymbol{V}_t$) and total impedance ($\boldsymbol{Z}_t$) of the motor, the current drawn by the motor $\boldsymbol{I}_s$ is

$$\mathbf{I}_s = \frac{\mathbf{V}_t}{\mathbf{Z}_t} \tag{3.3}$$

where

$$\mathbf{Z}_t = \frac{(jX_m)\left(\dfrac{R_r}{s} + jX_r\right)}{\dfrac{R_r}{s} + j(X_r + X_m)} + \mathbf{Z}_s$$

The dynamic behavior of an induction motor can be represented by the following differential equation [3]

$$\frac{ds}{dt} = \frac{1}{2H}(T_m - T_e) \tag{3.4}$$

where H, T_m, T_e and s are the inertia constant, mechanical load torque, electrical developed torque and slip respectively, of the motor.

For a given terminal voltage, the air-gap power P_{ag} depends on motor parameters and operating slip. In per unit, the air-gap power P_{ag} is the same as the electrical developed torque T_e of the motor. Note that P_{ag} and hence electrical torque T_e depends on the quantities at point DD' (in Fig. 3.2).

In Fig. 3.2, the power absorbed by the resistance R_r/s represents the air-gap power and it can be expressed as

$$P_{ag} = \frac{R_r}{s} I_r^{\,2} = \frac{V_r^2}{R_r} s \tag{3.5}$$

Mechanical load torque T_m is assumed as follows

$$T_m = T_c + T_s s + T_q (1-s)^2 \tag{3.6}$$

where, T_c, T_s and T_q are the coefficients of the constant, static and quadratic components, respectively, of load torque. For short-term voltage stability investigations, static and quadratic components of mechanical load torque are considered as zero. For long-term voltage stability investigations all the components are considered.

3.2.2 Two Bus Equivalent of the Study System

P-V and *Q-V* curves are very commonly used to assess the voltage stability of a power system. Normally *P-V* curve is developed for a constant power factor. But at the motor terminals BB' in Fig 3.2, the power factor varies depending on the mechanical load on the motor. Further, the reactive power consumed by the induction motor also depends on the power factor at which it is operating. For such a situation, it is difficult to develop the *P-V* curve at the motor terminals BB'. However, at terminals DD' the power factor is always unity. In this study, the *P-V* curve is generated at a motor internal point DD' (across the resistance R_r/s). The power at resistance R_r/s represents the equivalent mechanical load on the motor. Therefore to develop the *P-V* curve, the active power (P) consumed by R_r/s is considered as load. *P-V* curves have successfully been used in many articles to assess the voltage stability limit [3, 5, 15,

16, 30-31, 49, 50]. In this case, the maximum load is determined from the nose point of the *P-V* curve. Note that at point DD', there is no reactive power (because there is no reactance in right side of point DD') and thus *Q-V* curve does not exit.

The circuit left of point DD' in Fig. 3.2 is represented by another Thevenin equivalent circuit having parameters of $\mathbf{V}'_{th}$ and $\mathbf{Z}'_{th}$. The power absorbed by R_r/s is represented by *P*. Such an equivalent circuit is shown in Fig. 3.3.

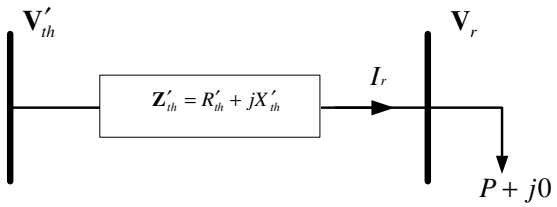

Fig. 3.3 Two-bus representation of the study system of Fig 3.2

Thevenin equivalent parameters $\mathbf{V}'_{th}$ and $\mathbf{Z}'_{th}$ are given by

$$\mathbf{V}'_{th} = \frac{\mathbf{V}_{th}(jX_m)}{\mathbf{Z}_{th} + \mathbf{Z}_l + \mathbf{Z}_s + jX_m} \tag{3.7}$$

$$\begin{aligned}\mathbf{Z}'_{th} &= \frac{(\mathbf{Z}_{th} + \mathbf{Z}_l + \mathbf{Z}_s)(jX_m)}{\mathbf{Z}_{th} + \mathbf{Z}_l + \mathbf{Z}_s + jX_m} + jX_r \\ &= R'_{th} + jX'_{th}\end{aligned} \tag{3.8}$$

The complex voltage equation of the circuit of Fig. 3.3 can be written as

$$\mathbf{V}'_{th} = \mathbf{V}_r + (\frac{P - j0}{\mathbf{V}_r^*})\mathbf{Z}'_{th} \tag{3.9}$$

$$\mathbf{V}'_{th}\mathbf{V}_r^* = \mathbf{V}_r\mathbf{V}_r^* + PR'_{th} + jPX'_{th}$$

When $\mathbf{V}_r$ is considered as reference, the above equation becomes

$$\mathbf{V}'_{th}V_r = V_r^2 + PR'_{th} + jPX'_{th} \tag{3.10}$$

Magnitude of the above complex equation can be expressed as

$$\left|\mathbf{V}'_{th}V_r\right| = \left|\left(V_r^2 + PR'_{th}\right) + jPX'_{th}\right|$$

or

$$V_r^4 + \left(2R'_{th}P - V'^2_{th}\right)V_r^2 + P^2\left(R'^2_{th} + X'^2_{th}\right) = 0 \qquad (3.11)$$

This can be written as

$$aV_r^4 + bV_r^2 + c = 0 \qquad (3.12)$$

where $a = 1,\ b = 2R'_{th}P - V'^2_{th},\ c = P^2\left(R'^2_{th} + X'^2_{th}\right)$

Note that for a given motor, the Thevenin parameters (R'_{th}, V'_{th} and X'_{th}) are constant and independent of motor operating point. Equation (3.12) is a fourth order equation and mathematically it has four possible solutions. By considering $x = V_r^2$, equation (3.12) can be written as following quadratic form

$$ax^2 + bx + c = 0 \qquad (3.13)$$

The solutions of equation (3.13) are

$$x_1 = \frac{-b + \sqrt{d}}{2a} \quad \text{and} \quad x_2 = \frac{-b - \sqrt{d}}{2a} \qquad (3.14)$$

where

$$\begin{aligned} d &= b^2 - 4ac \\ &= \left(2R'_{th}P - V'^2_{th}\right)^2 - 4P^2\left(R'^2_{th} + X'^2_{th}\right) \\ &= P^2\left(-4X'^2_{th}\right) + P\left(-4R'_{th}V'^2_{th}\right) + V'^4_{th} \end{aligned}$$

Thus, the four possible solutions of V_r are

$$V_{r1} = +\sqrt{x_1} = +\sqrt{\frac{-b + \sqrt{d}}{2a}},\quad V_{r2} = +\sqrt{x_2} = +\sqrt{\frac{-b - \sqrt{d}}{2a}}\ ; \qquad (3.15a)$$

$$V_{r3} = -\sqrt{x_1} = -\sqrt{\frac{-b + \sqrt{d}}{2a}}\ ;\ V_{r4} = -\sqrt{x_2} = -\sqrt{\frac{-b - \sqrt{d}}{2a}}\ ; \qquad (3.15b)$$

Note that V_r is voltage magnitude and it should be a real and positive number. Thus, solutions V_{r3} and V_{r4} are not feasible at all, but the solutions V_{r1} and V_{r2} are feasible under certain conditions which are described below.

Note that $b = 2R'_{th}P - V'^{2}_{th}$ and $d = P^2\left(-4X'^{2}_{th}\right) + P\left(-4R'_{th}V'^{2}_{th}\right) + V'^{4}_{th}$. At no load ($P = 0$), $b = -V'^{2}_{th}$ and $d = V'^{4}_{th}$. Thus $V_{r1} = V'_{th}$ and $V_{r2} = 0$, that is at least one of the solutions of equation (3.12) is positive because V'_{th} is a positive number. When the motor power P is increased, b increases from $-V'^{2}_{th}$ but it remains negative in the entire operating range of P ($0 \le P \le 1$) because $R'_{th} << V'^{2}_{th}$. At the same time, *d* decreases from V'^{4}_{th} and eventually it becomes zero at the maximum or critical power point. If P is increased further, *d* becomes negative and that will provide complex values of V_{r1} and V_{r2}, which are not feasible indicating that the motor has already entered the voltage instability region. Within the voltage stability region ($d > 0$), the solution that has higher value (V_{r1}) is called the stable solution V_s and the lower value of solution (V_{r2}) is called unstable solution V_u [31, 49].

Thus

$$V_s = V_{r1} = \sqrt{\frac{-b + \sqrt{d}}{2a}} \tag{3.16}$$

$$V_u = V_{r2} = \sqrt{\frac{-b - \sqrt{d}}{2a}} \tag{3.17}$$

The above two solutions are used to plot the *P-V* curve of the system [50]. At no load ($P = 0$), $V_s = V'_{th}$ and $V_u = 0$. As the load increases, V_s decreases and V_u increases as can be seen in Fig. 3.4. At the voltage collapse point both the solutions become the same because $d = 0$.

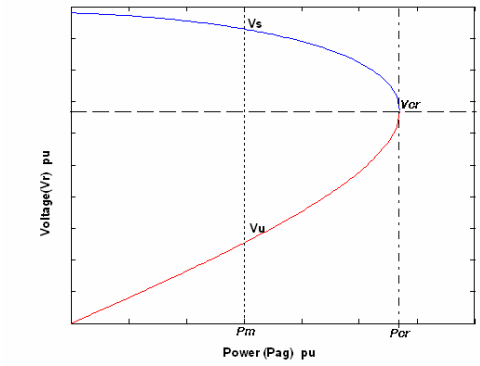

Fig. 3.4 Network *P-V* curves

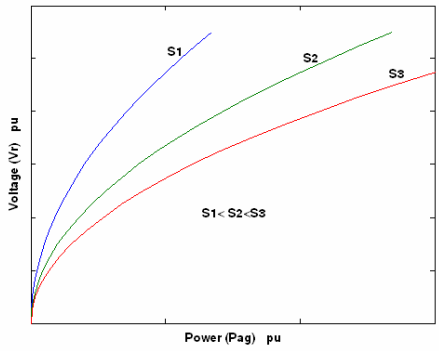

Fig. 3.5 Motor *P-V* curves

The network *P-V* curves, shown in Fig 3.4, are developed as follows

Step 1 Initially assume the value of P as zero

Step 2 Compute V_s and V_u using the expressions (3.16) and (3.17)

Step 3 Increase the value of P by a small increment and repeat step 2 until d becomes zero.

When the load P is increased, the system ultimately reaches the voltage collapse point, where both V_s and V_u approaches to the same value (i.e., when d = 0, $V_s = V_u$) and is called critical voltage (V_{cr}) and the corresponding power is called the critical power (P_{cr}).

From equation (3.5), for a given slips, the air-gap power P_{ag} of an induction motor depends on the voltage V_r. The variation of P_{ag} against V_r can be considered as the P-V curve of the motor (for a constant slip) at point DD' and is also shown in Fig. 3.5.

To satisfy the power balance criterion at point DD', the system must operate at the point of intersection of the motor and network P-V curves. The power at the point of intersection represents the power at points DD' of Fig. 3.2 and it also represents the air-gap power of the motor. If the rotor copper loses is assumed negligible then the electrical power of the motor will be equal to the mechanical load on the motor. The above concept is used to verify the stability of the motor as well as to determine the new stable operating point following a disturbance.

3.2.3 Line Outage

Consider that one of the lines in Fig. 3.1 is suddenly tripped and that would change the Thevenin parameters of Fig. 3.3 and hence the P-V curves of the network. Fig. 3.6 shows the network P-V curve before and after the line outage. Assume that the motor delivers a constant power of P_m as shown by a vertical line in Fig 3.6. The corresponding initial operating point is 'a' with slip s_1 (with double line). When one of the lines is taken away, the motor will ultimately operate at point 'c' (on curve II) to satisfy the same power requirement. The motor P-V curve that passes through point 'c' has a slip of s_2. However, the motor speed or slip cannot change instantaneously. In this case, the motor operating point first suddenly jumps from point 'a' (on curve I) to point 'b' (on curve II) at the same slip, this happen at the instant of line outage. At

point '*b*', motor power is less than the load power and thus the motor decelerates and slip increases. Thus the operating point starts moving along the post disturbed network *P-V* curve (curve II) until it reaches the new stable equilibrium point '*c*'. If the initial load of the motor is greater than P_{cr2}, there will be no point of intersection of the motor power and the post disturbed network *P-V* curve and hence no stable operating point can be reached following the line outage and finally the motor will stall.

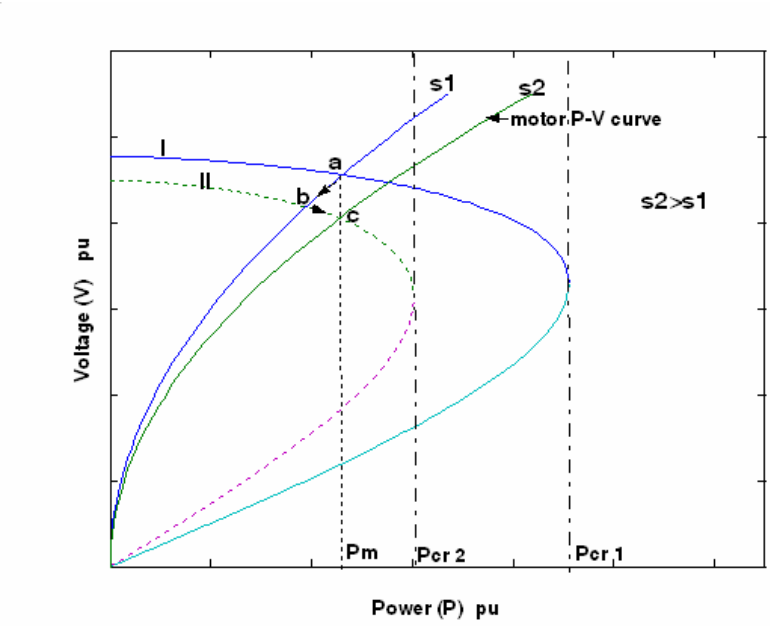

Fig. 3.6 Illustration of network and motor *P-V* curves, I: with double line; II: with single line

One of the possible ways to operate the motor at higher load levels with a feasible post disturbed stable operating point is by shifting the nose point of the network *P-V* curve (or the critical power P_{cr}) towards the right. This can be achieved by reducing the Thevenin impedance through adding a shunt capacitor at the motor terminals BB' (in Fig. 3.2). The shunt capacitor changes the Thevenin parameters and hence the *P-V* curve, which is illustrated in Fig. 3.7 (curve III). Consider that the motor is now operating at a higher load levels (at point '*d*') and due to line outage the operating point suddenly moves to point '*e*' and then travel along the *P-V* curve II. When the shunt capacitor is added, the operating point again suddenly moves from point '*f*' (on curve II) to point '*g*' (on curve III obtained with shunt capacitor). At point '*g*', motor power is higher than the load power and thus it accelerates and ultimately reaches the

stable equilibrium point '*h*'. Without the shunt capacitor, the motor operating point moves along the *P-V* curve II (following the line outage) and it cannot reach the pre-disturbed power level of P_{m2} and thus it stalls. If switching of the capacitor is delayed (after reaching a slip of s_4 at which P_{m2} and *P-V* curve III intersect), the motor may not reach the stable equilibrium point '*h*'. In this case, the motor power (when the capacitor is switched on) will reach to a value of less than the load power and that would cause to decelerate the motor further.

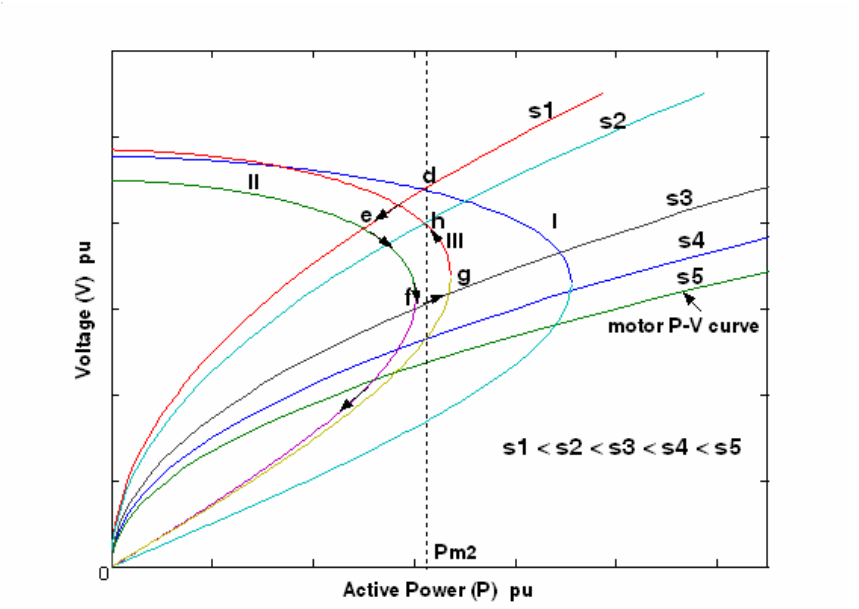

Fig. 3.7 Illustration of network and motor *P-V* curves, I: with double line; II: with single line; III: single line with capacitor at motor terminals

3.2.4 3-Phase Fault

For a 3-phase fault at the motor terminal, the voltage as well as the motor power becomes zero. In this case, the motor operating point suddenly moves from initial operating point '*d*' in Fig. 3.8 to the origin (zero power) and then starts decelerating. Consider that the fault is cleared (by opening one of the lines) when the motor slip increases to s_3. Thus, at fault clearing the operating point will suddenly moves from origin to point '*j*' where the motor power is higher than the load power. Thus the motor starts accelerating and ultimately it will reach the stable operating point '*f*'. If the fault clearance is delayed (when the motor slip reaches s_4) the operating point will suddenly moves from origin to the point '*k*' where the motor power is equal to the

load power. This represents the critical situation. However, if the fault clearance is further delayed, the motor slip increases beyond s_4 where the motor power is less than the load power at fault clearing. Thus motor starts decelerating causing increase in the slip further and finally it stalls. Therefore the operating point '*k*' (point at which P_m and *P-V* curve *III* intersect at slip s_4) is called the critical slip (s_{cr}). From the above discussion it is of curiosity to investigate and determine the critical fault clearing time for which the motor ultimately reaches a stable operating point.

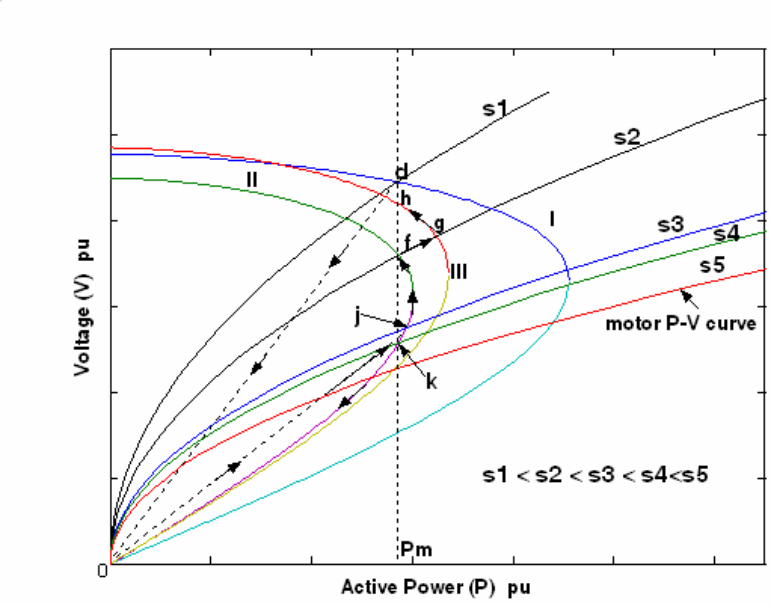

Fig. 3.8 Illustration of network and motor *P-V* curves, I: with double line; II: with single line; III: single line with capacitor at motor terminals

When a shunt capacitor is added to the motor terminals, same as the previous line outage case, there will be changes in the Thevenin parameters. The operating point again suddenly moves from point '*f*' (on curve *II*) to point '*g*' (on curve *III* obtained with shunt capacitor). At point '*g*', motor power is higher than the load power and thus it accelerates and ultimately reaches a new stable equilibrium point '*h*'.

3.2.5 Determination of Critical Fault Clearing Time (t_{cr})

In this section a method for determining the critical fault clearing time to avoid the stalling of induction motor load due to a 3-phase fault at the motor terminals is described.

The dynamics of the induction motor can be expressed as

$$\frac{ds}{dt} = \frac{1}{2H}(T_m - T_e)$$

For a 3-phase fault at the terminals of the induction motor, the terminal voltage of the motor becomes zero and thus the torque developed by the motor (T_e) is also becomes zero. Therefore, the dynamics of the motor during faulted period is govern by the following differential equation

$$\frac{ds}{dt} = \frac{1}{2H}(T_m) \tag{3.18}$$

Integrate both sides of equation (3.18) with respect to time

$$\int\left(\frac{ds}{dt}\right)dt = \int\left(\frac{1}{2H}T_m\right)dt \tag{3.19}$$

When the load torque (T_m) is considered as constant, the slip of the motor during the faulted period can be expressed as

$$s = \frac{T_m}{2H}t + C \tag{3.20}$$

At pre-fault condition, i.e. at $t = 0$, $s = s_0$ and thus $C = s_0$. Substituting C in expression (3.20)

$$s = \frac{T_m}{2H}t + s_0 \tag{3.21}$$

The time at which the motor slip reaches the critical slip (s_{cr}) is defined as the critical fault clearing time (t_{cr}).

$$s_{cr} = \frac{T_m}{2H}t_{cr} + s_0 \tag{3.22}$$

From equation (3.22), the value of t_{cr} can be written as

$$t_{cr} = \frac{2H}{T_m}(s_{cr} - s_0) \tag{3.23}$$

3.2.6 Determination of Critical Slip (s_{cr})

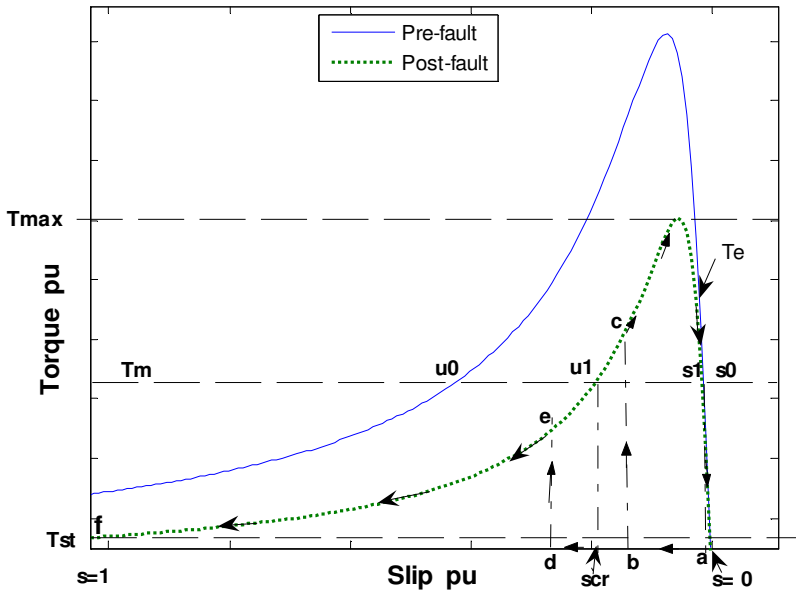

Fig. 3.9 Torque-slip characteristics of induction motor

Torque slip characteristics of the motor for pre-fault (solid line) and post fault (dotted line) conditions are shown in Fig. 3.9. The constant mechanical load torque on the motor is shown by a dashed line parallel to slip axis. The stable operating slips (s_0 and s_1) as well as the unstable operating slips (u_0 and u_1) for pre-fault and post-fault conditions are also shown in Fig. 3.9. When a 3-phase fault occurs in the system, voltage as well as electrical torque developed by the motor becomes zero and thus the operating point suddenly jump from 's_0' to 'a'. During faulted period, the motor decelerates and thus the slip increases along *a-b*. If the fault is cleared rapidly before the slip reaching the unstable equilibrium value 'u_1' in Fig. 3.9, T_e developed by the motor is more than the T_m and thus the motor accelerates and finally reaches a stable equilibrium point 's_1' i.e., operating point moves along the path of 's_0-*a*-*b*-*c*-s_1'. If the fault clearing is delayed beyond point 'u_1', T_e developed by the motor is less than the T_m, the motor will decelerate further and finally i.e. operating point moves along the path of 's_0-*a*-*b*-*d*-*e*-*f*'. Therefore the slip corresponding to point 'u_1' is equal to the

critical slip (s_{cr}) that is same as operating point '*k*' in the Fig 3.8 where P_e is equal to P_m at slip s_4.

The electrical torque T_e depends on the quantities at point DD' (in Fig. 3.2) and it is same as P in Fig 3.3 and which can be expressed as

$$T_e = \frac{R_r}{s} I_r^2 \tag{3.24}$$

the rotor current (I_r) can be written as

$$I_r = \left| \frac{\mathbf{V}'_{th}}{\mathbf{Z}'_{th} + \frac{R_r}{s}} \right| = \left| \frac{\mathbf{V}'_{th}}{\left(R'_{th} + \frac{R_r}{s} \right) + j\left(X'_{th} \right)} \right|$$

Thus the motor torque T_e of equation (3.24) becomes

$$T_e = \frac{(V'_{th})^2}{\left(R'_{th} + \frac{R_r}{s} \right)^2 + (X'_{th})^2} \frac{R_r}{s} \tag{3.25a}$$

At the critical slip or unstable point T_m is equal to T_e, therefore the equation (3.25a) can also be written as

$$T_e = T_m = \frac{(V'_{th})^2}{\left(R'_{th} + \frac{R_r}{s} \right)^2 + (X'_{th})^2} \frac{R_r}{s} \tag{3.25b}$$

Equation (3.25b) is simplified further and expressed as

$$s^2 \left(R'^2_{th} + X'^2_{th} \right) + s \left(2R'_{th} R_r - \frac{V'^2_{th} R_r}{T_m} \right) + R_r^2 = 0$$

The above expression can be written as

$$C_1 s^2 + C_2 s + C_3 = 0 \tag{3.26}$$

where $C_1 = R'^2_{th} + X'^2_{th}$, $C_2 = 2R'_{th} R_r - \frac{V'^2_{th} R_r}{T_m}$, $C_3 = R_r^2$

Note that for a given motor, the parameters R_r, R'_{th}, V'_{th} and X'_{th} are constant and

independent of motor operating point.

Equation (3.26) has two possible solutions,

$$s_{1,2} = \frac{-C_2 \pm \sqrt{d_1}}{2C_1} \tag{3.27}$$

where

$$d_1 = C_2^2 - 4C_1C_3$$

$$= \left(2R'_{th}R_r - \frac{V'^2_{th}R_r}{T_m}\right)^2 - 4\left(R'^2_{th} + X'^2_{th}\right)\left(R_r^2\right)$$

After simplification

$$d_1 = (V'^4_{th}R_r^2)\frac{1}{T_m^2} - \frac{1}{T_m}\left(4R'_{th}R_r^2V'^2_{th}\right) - \left(4X'^2_{th}R_r^2\right)$$

When T_m is very small (during light load conditions), $C_2 < 0$ and $d_1 > 0$. Thus at least one of the solutions of s is positive. As T_m (or load) increases, C_2 increases and d_1 decreases and eventually s becomes non positive (either negative or complex) and that occurs at the critical load. If the value of d_1 becomes negative, solutions of the equation (3.27) become complex and which are considered as infeasible solutions as the induction motor slip should be within the range of 0 to 1.

The variation of motor electrical torque (T_e) against slip (s) is shown in Fig. 3.9 by dotted line. The constant mechanical load torque (T_m) is also shown in Fig. 3.9 by dashed lines. Equation (3.27) provides the value of slip at $T_m = T_e$ as described by equation (3.25b). Graphically, the slip can also be obtained from the point of intersections of T_m line and T_e curve as shown in Fig. 3.9. When $T_{st} < T_m < T_{\max}$, there are two point of intersections (U_1 and S_1) as can be seen in Fig. 3.9 indicating that equation (3.27) will provide two feasible solutions. From the induction motor theory, lower value of slip (S_1) is called stable solution while higher value of slip (U_1) is called unstable solution. When $T_m > T_{\max}$, there is no point of intersection of T_m line and T_e curve in Fig. 3.9 indicating that equation (3.27) will not provide any feasible solution. However, when $T_m < T_{st}$, there is only one point of intersection of T_m line

and T_e curve in Fig. 3.9 and thus equation (3.27) will provide only one feasible value of slip.

3.3 Long-Term Voltage Stability

This section investigates the phenomenon of long-term voltage stability of a power system by considering the dynamics of both fast and slow-acting devices. In general, the fast-acting devices reached the quasi steady-state equilibrium point before the start of operation of the slow-acting devices.

3.3.1 Study System and its Mathematical Model

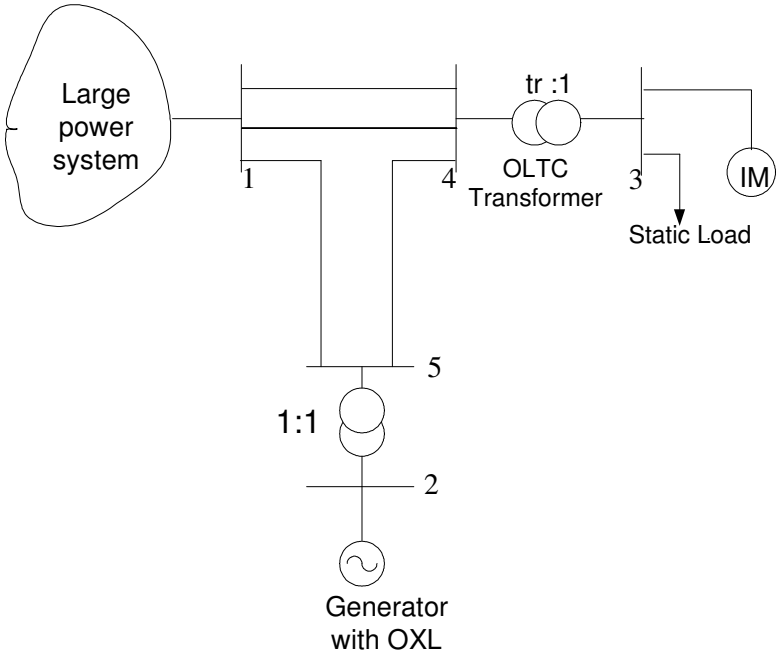

Fig. 3.10 Single line diagram of a simple power system for long-term voltage stability

Consider a local load bus is supplied by a large power system through a double circuit transmission lines and an OLTC transformer as shown in Fig. 3.10. At bus 2, a generator is connected to the system to supply part of the demand and support bus voltages. The system loads are represented by an aggregated induction motor load and an exponential load. The large power system is represented by its Thevenin equivalent

circuit consisting of a fixed voltage source behind the Thevenin impedance. The local generator at bus 2 in Fig. 3.10 has been represented with the AVR and OXL. The objective of this study is to investigate the effect of slow acting devices, such as generator OXL and OLTC transformer on dynamic voltage stability of the system. The equivalent circuit of the study system is shown in Fig. 3.11. Large power system is represented with its fixed thevenin equivalent source ($E_{th}\angle\theta_{th}$) behind the series reactance (X_{th}). Transmission lines are represented with their equivalent reactance X_{ij} . Transformers are represented by their equivalent π circuit model. The transformer between buses 2 and 5 is considered as fixed turns ratio transformer. The transformer between buses 4 and 3 is considered with an OLTC.

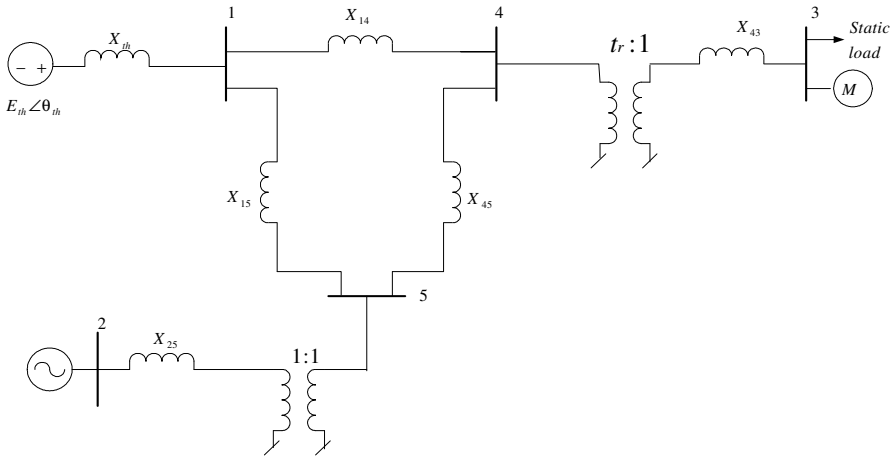

Fig.3.11 Equivalent circuit representation of Fig 3.10

The mathematical model of various components of the system apart from the induction motor (which has already been discussed in Section 3.2.1) is briefly described in the following sections.

3.3.2 Generator Model

The dynamics of the generator are represented by a set of differential equations as shown below [3]:

$$\frac{d\delta}{dt} = \omega \tag{3.28}$$

$$\frac{d\omega}{dt} = \frac{\omega_0}{2H}\left(P_m - P_g\right) - \frac{D}{2H}\omega \tag{3.29}$$

$$\frac{dE'_q}{dt} = \frac{-E'_q + v_{fd} - \left(X_d - X'_q\right)i_d}{T'_{do}} \tag{3.30}$$

where δ, ω, D, H, P_m and P_g are the rotor angle, speed, damping coefficient, inertia constant, input mechanical power and output electrical power of the generator respectively. E'_q, v_{fd}, T'_{do} and id are the voltage behind the transient reactance, field voltage seen by the armature, open circuit transient time constant and direct axis armature current, respectively. X_d, X_q are the direct and quadratic axis reactance, respectively, and X'_d is direct axis transient reactance.

Complex power delivered by the generator in *x-y* (real and imaginary) reference frame is

$$\mathbf{S}_g = P_g + jQ_g = \mathbf{V}_g \mathbf{I}_g^* \tag{3.31}$$

where $\mathbf{V}_g = v_{gx} + jv_{gy}$ is the terminal voltage of the generator, $\mathbf{I}_g = i_{gx} + ji_{gy}$ is the current supplied by the generator.

In general, the generator differential equations are represented in *d-q* reference frame and network equations are in *x-y* reference frame. Thus it is necessary to convert quantities from one reference frame to another reference frame.

The current in *d-q* reference frame can be obtained from the following expression

$$\begin{bmatrix} i_d \\ i_q \end{bmatrix} = \mathbf{T}^{-1} \begin{bmatrix} i_{gx} \\ i_{gy} \end{bmatrix} \tag{3.32}$$

where

$$\mathbf{T} = \begin{bmatrix} \sin\delta & \cos\delta \\ -\cos\delta & \sin\delta \end{bmatrix} \text{ and } \mathbf{T}^{-1} = \begin{bmatrix} \sin\delta & -\cos\delta \\ \cos\delta & \sin\delta \end{bmatrix}$$

From equation (3.32) i_d can be written as

$$i_d = i_{gx}\sin\delta - i_{gy}\cos\delta \tag{3.33}$$

Stator voltage equations in *d-q* reference frame are expressed as [3]

$$\begin{bmatrix} v_d \\ v_q \end{bmatrix} = \begin{bmatrix} 0 & X_q \\ -X'_d & 0 \end{bmatrix} \begin{bmatrix} i_d \\ i_q \end{bmatrix} + \begin{bmatrix} 0 \\ E'_q \end{bmatrix} \tag{3.34}$$

Stator voltage equations (3.34) in *x-y* reference frame can be expressed as [3]

$$\begin{bmatrix} v_{gx} \\ v_{gy} \end{bmatrix} = \mathbf{T} \begin{bmatrix} v_d \\ v_q \end{bmatrix} = \mathbf{T} \begin{bmatrix} 0 & X_q \\ -X'_d & 0 \end{bmatrix} \mathbf{T}^{-1} \begin{bmatrix} i_{gx} \\ i_{gy} \end{bmatrix} + \mathbf{T} \begin{bmatrix} 0 \\ E'_q \end{bmatrix} \tag{3.35a}$$

Stator current equations in *x-y* reference frame can be expressed as

$$\begin{bmatrix} i_{gx} \\ i_{gy} \end{bmatrix} = \mathbf{T} \begin{bmatrix} 0 & 1/X'_d \\ -1/X_q & 0 \end{bmatrix} \mathbf{T}^{-1} \left\{ \begin{bmatrix} v_{gx} \\ v_{gy} \end{bmatrix} - \mathbf{T} \begin{bmatrix} 0 \\ E'_q \end{bmatrix} \right\} \tag{3.35b}$$

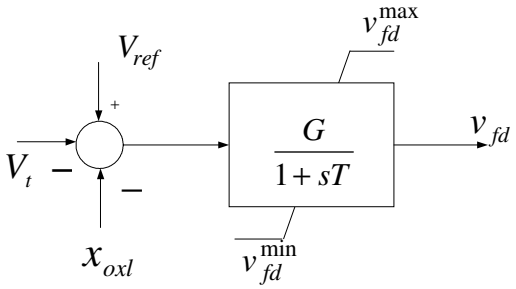

Fig. 3.12 Block diagram of *AVR*

Fig. 3.12 shows the AVR model of the generator [3]. The equations of the *AVR* model are given by

$$\begin{aligned} \frac{dv_{fd}}{dt} &= 0 && \text{if} \quad v_{fd} = v_{fd}^{\max} \quad \text{and} \quad G\left(V_{ref} - V_t - x_{oxl}\right) - v_{fd} > 0 \\ &= 0 && \text{if} \quad v_{fd} = v_{fd}^{\min} \quad \text{and} \quad G\left(V_{ref} - V_t - x_{oxl}\right) - v_{fd} < 0 \\ &= \frac{G\left(V_{ref} - V_t - x_{oxl}\right) - v_{fd}}{T} && \text{otherwise} \end{aligned} \tag{3.36}$$

where G and T are the gain and time constants of the voltage regulator respectively. The minimum and maximum field voltages are represented by $v_{fd}^{\min}$ and $v_{fd}^{\max}$,

respectively. V_t and V_{ref} are the generator terminal voltage and reference voltage of the AVR respectively. X_{oxl} is the output of the OXL.

Generator field winding can be protected from overheating by using OXL. The OXL usually tolerates a certain amount of overload for a short time and then forces to reduce the field current to the limiting value. In this study, the OXL with integral control of field current shown in Fig. 3.13 is considered [3]. In Figure 3.13, i_{fd} is the generator field current, $I_{fd}^{\lim}$ is the generator field current limit, S_1 and S_2 are positive slopes, K_1, K_2, K_r and K_i are positive gains, and X_{oxl} is the output of the OXL.

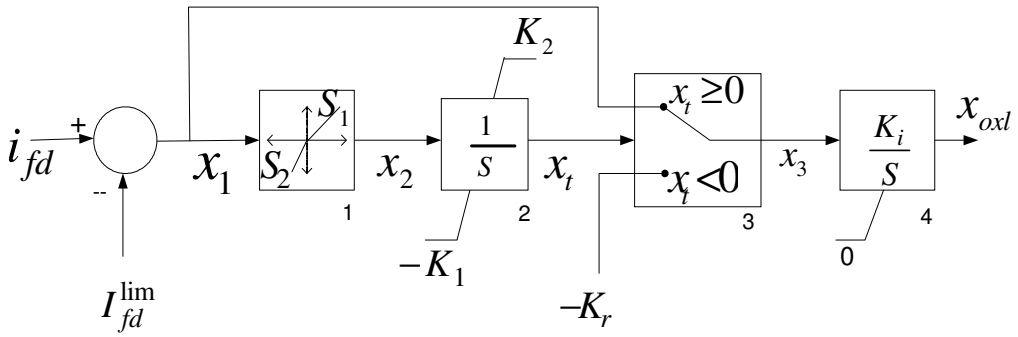

Fig. 3.13 Block diagram of an integral type OXL

The OXL input field current i_{fd} is by virtue the same as E_q in per unit. E_q can be expressed as [3]

$$E_q = E_q' + (X_d - X_d')i_d \tag{3.37}$$

In Fig. 3.13 the intermediate variable x_2 given as

$$\begin{aligned} x_2 &= S_1\left(E_q - I_{fd}^{\lim}\right) \quad if \quad Eq \geq I_{fd}^{\lim} \\ &= S_2\left(E_q - I_{fd}^{\lim}\right) \quad otherwise \end{aligned} \tag{3.38}$$

with $S_1, S2 > 0$, the state equation of block 2 (in Fig. 3.13) is given by,

$$\begin{aligned} \frac{dx_t}{dt} &= 0 \quad if \quad x_t = K_2 \ \ and \ \ x_2 \geq 0 \\ &= 0 \quad if \quad x_t = -K_1 \ \ and \ \ x_2 < 0 \\ &= x_2 \quad otherwise \end{aligned} \tag{3.39}$$

The intermediate variable x_3 is defined as follows

$$\begin{aligned} x_3 &= \left(E_q - I_{fd}^{\lim}\right) \qquad if \quad x_t \geq 0 \\ &= -K_r \qquad otherwise \end{aligned} \tag{3.40}$$

The OXL output X_{oxl} is given by following state equation

$$\begin{aligned} \frac{dx_{oxl}}{dt} &= 0 \qquad if \quad x_{oxl} = 0 \;\; and \;\; x_3 \geq 0 \\ &= K_i \, x_3 \qquad otherwise \end{aligned} \tag{3.41}$$

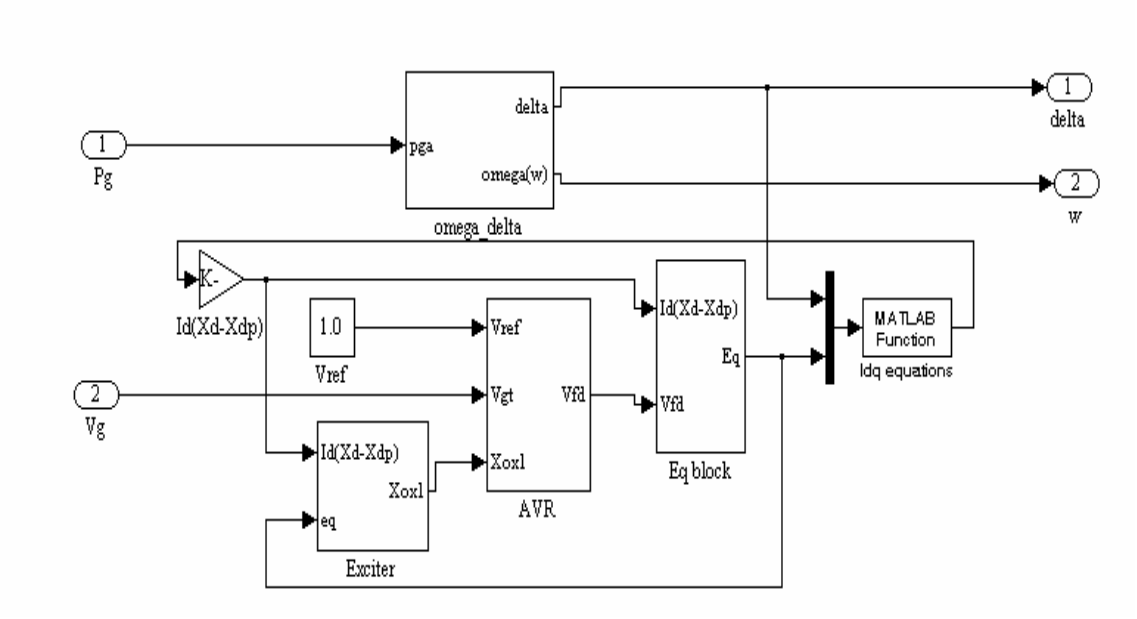

Fig. 3.14 SIMULINK block diagram of generator

The block diagram of the generator with input variables and output variables is shown in Fig. 3.14. In Fig 3.14 input variables (P_g, V_g) are obtained from the stator algebraic equations and output state variables are obtained from dynamic equations of generator, AVR and OXL.

3.3.3 On Load Tap Changer Transformer Model

The block diagram of OLTC transformer model is shown in the Fig. 3.15 [1, 2, 3, 27]. The main objective of the OLTC is to adjust the turn's ratio of the transformer in order to maintain voltage within the limits in spite of the voltage variations of the

transmission system. For long-term dynamics, voltage control by OLTC transformers may need to be modeled.

In each step, the change in turn ratio depends on the voltage difference (ΔV) between the actual voltage (V_3) and reference voltage (V_{ref}) and sum of the tolerance (ε) and dead band (D).

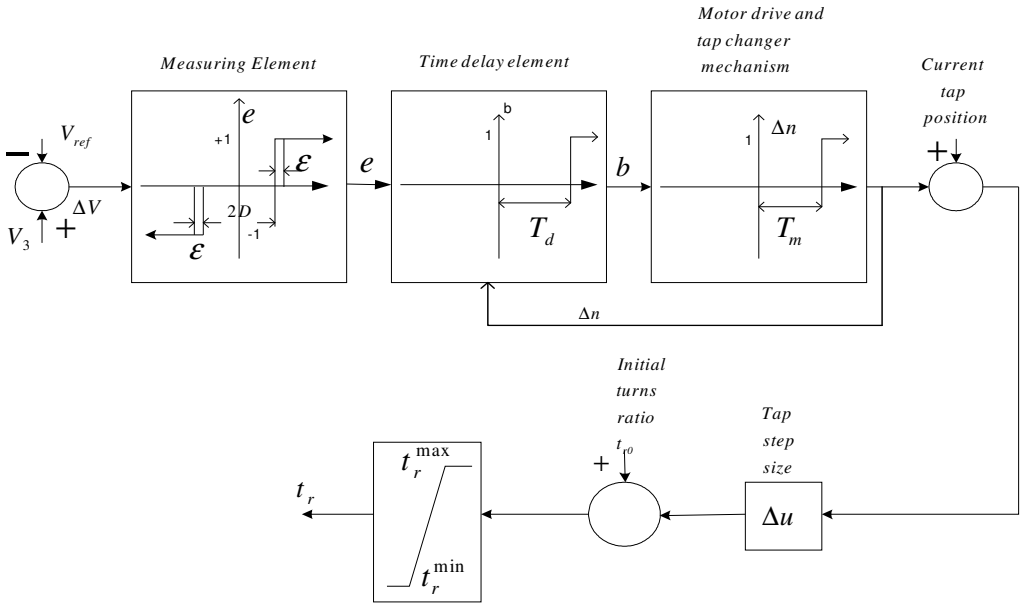

Fig. 3.15 Block diagram representation of the On Load Tap Changer (OLTC)

Equation (3.42) gives the response of the measuring element

$$\begin{aligned} e &= +1 \quad \text{for } \Delta V > D + \varepsilon \\ &= -1 \quad \text{for } \Delta V < -(D + \varepsilon) \\ &= 0 \quad \text{otherwise} \end{aligned} \tag{3.42}$$

The response of the time delay (T_d) element can be represented by the following equation

$$\begin{aligned} T_d &= T_d \quad \text{for the first step} \\ &= T_m \quad \text{for sub sequent steps} \end{aligned} \tag{3.43}$$

Output of the time delay element (b) is as follows

$$\begin{aligned} b &= +1 \quad \text{for } t > T_d \quad \text{and} \quad e = +1 \\ &= -1 \quad \text{for } t > T_d \quad \text{and} \quad e = -1 \\ &= 0 \quad \text{otherwise} \end{aligned} \tag{3.44}$$

The response of the motor drive and tap changer mechanism is given by the following equation.

$$\begin{aligned} \Delta n &= +1 \quad for\ t > T_m \quad and \quad b = +1 \\ &= -1 \quad for\ t > T_m \quad and \quad b = -1 \\ &= 0 \qquad otherwise \end{aligned} \tag{3.45}$$

Tap position is the sum of the current tap position and the size of the tap increment Δn i.e,

$$n_i = current\ tap\ position\ (n_{i-1}) + \Delta n$$

The turn's ratio of the OLTC is

$$t_r = initial\ turns\ ratio + \Delta u * n_i \tag{3.46}$$

$$if \qquad t_r^{\min} < t_r < t_r^{\max}$$

where Δu is the incremental change in turns ratio, $t_r^{\min}$ and $t_r^{\max}$ are minimum and maximum turns ratio of the OLTC transformer respectively.

The expression (3.46) gives the turn ratio (t_r) of the OLTC transformer as a discrete variable that varies in steps with an initial delay of T_d and subsequent delay of T_m. The operating time T_n for the n-th step of OLTC can be expressed as

$$T_n = T_d + (n-1)T_m \tag{3.47}$$

3.3.4 Exponential Load Model

The exponential loads of the system are considered as voltage dependent and represented by the following exponential form [3]

$$\begin{aligned} P_{sl} &= P_0 \left(\frac{V}{V_0} \right)^a \\ Q_{sl} &= Q_0 \left(\frac{V}{V_0} \right)^b \end{aligned} \tag{3.48}$$

Here P_0 and Q_0 are the active and reactive powers consumed by the exponential load at a nominal voltage of V_o.

Note that equation (3.48) represents generalized exponential load model. For constant impedance load model, P_{sl} and Q_{sl} are proportional to the square of load voltage. For such a case the values of a and b are 2. For constant current load model, P_{sl} and Q_{sl} are proportional to load voltage and thus the values of a and b are 1. For constant power load model P_{sl} and Q_{sl} are constant and independent of voltage, so values of a and b are 0. In this study, constant impedance load model is used and for which a = b = 2.

Current drawn by load is given by

$$\mathbf{I}_{sl} = \frac{P_{sl} - jQ_{sl}}{V_t^*} \tag{3.49}$$

where P_{sl}, Q_{sl} are the real and reactive powers drawn by the load.

3.3.5 Network Equations

The active and reactive power balance equations at bus i of the network shown in Fig. 3.10 can be written as.

$$\begin{aligned} P_{gi} - P_{Li} - V_i \sum_{k=1}^{n} V_k \left(G_{ik} \cos\theta_{ik} + B_{ik} \sin\theta_{ik}\right) = 0 \\ Q_{gi} - Q_{Li} - V_i \sum_{k=1}^{n} V_k \left(G_{ik} \sin\theta_{ik} - B_{ik} \cos\theta_{ik}\right) = 0 \end{aligned} \tag{3.50}$$

Here n is the total number of buses and $\mathbf{Y} = G+jB$ is the admittance matrix of the system. P_{Li} and Q_{Li} are the active and reactive components of load (sum of exponential and induction motor load) of bus i. P_{gi} and Q_{gi} are the active and reactive components of the generated power at bus i. V_i and θ_i are the voltage magnitude and phase angle of bus i.

In determining the admittance matrix, the transformers are represented by nominal π-circuit model as shown in Fig. 3.16 [3, 51]. Representation of the transformers with 1: t_r off nominal tap setting is as follows

where

$$\mathbf{Y}_{ij} = \left(\frac{1}{t_r}\right)\mathbf{Y}_t \tag{3.51}$$

$$\mathbf{Y}_{ij1} = \left(\frac{t_r - 1}{t_r} \right) \mathbf{Y}_t \tag{3.52}$$

$$\mathbf{Y}_{ij2} = \left(\frac{1 - t_r}{t_r^2} \right) \mathbf{Y}_t \tag{3.53}$$

Here $\mathbf{Y}_t$ is the transformer admittance.

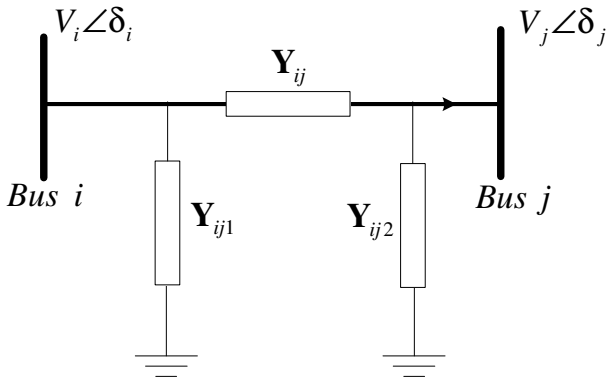

Fig. 3.16 Equivalent circuit of a transformer with off nominal taps setting of 1: t_r

3.4 Simulation Modeling

The MATLAB/SIMULINK model for short-term voltage stability of the system (Fig. 3.2) is shown in Fig. 3.17. In this case, all the algebraic equations (3.1) to (3.17) apart from equation (3.4) (which is induction motor dynamic equation) were implemented in 'm-file'.

The computational steps to investigate the short-term voltage stability for the system Fig 3.2 are given in the following

Step 1 Assume the initial slip as 1.

Step 2 Determine the motor stator current I_s and rotor current I_r from Fig 3.2.

Step 3 Calculate V_r, which is the product of I_r and R_r/s.

Step 4 Calculate V_t using the equation (3.2).

Step 5 Calculate the active power consumed (P_{ag}) by the rotor resistance using

equation (3.5), and then determine the slip of the induction motor using equation (3.4).

Step 6 Repeat steps 2 to 4 using the slip determined in step 4 for a sufficiently long time.

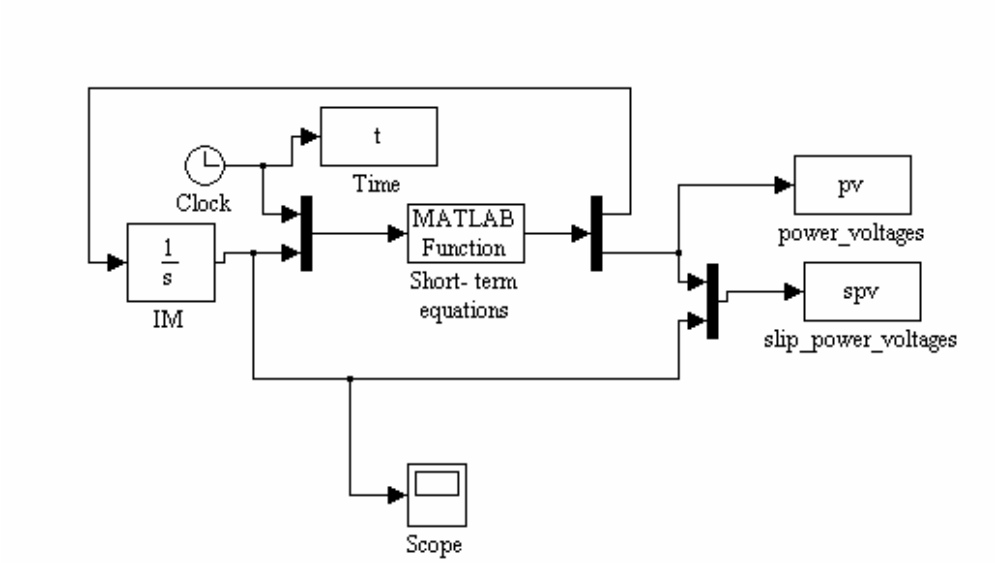

Fig. 3.17 SIMULINK/MATLAB block diagram for short-term voltage stability

Fig 3.18 shows the SIMULINK/MATLAB block diagram used for long-term time domain simulations as per the steps described earlier. In this case algebraic equations of all the components were incorporated in '*m-file*' and dynamic equations of the components were represented by SIMULINK blocks.

The computational steps to investigate the long-term voltage stability for the system shown in Fig 3.10 are given in the following

Step1 Define the system parameters (network parameters, generator parameters, load parameters, induction motor parameters) and assume initial bus voltages as unity.

Step 2 Use state variables coming from SIMULINK blocks (Eq, δ, s and t_r) to construct T matrix and its inverse, to compute the induction motor equivalent impedance, load torque, Y matrix and Z matrix.

Step 3 Calculate the current injections and bus voltage vectors.

Step 4 Repeat steps 2 and 3 for a sufficiently long time.

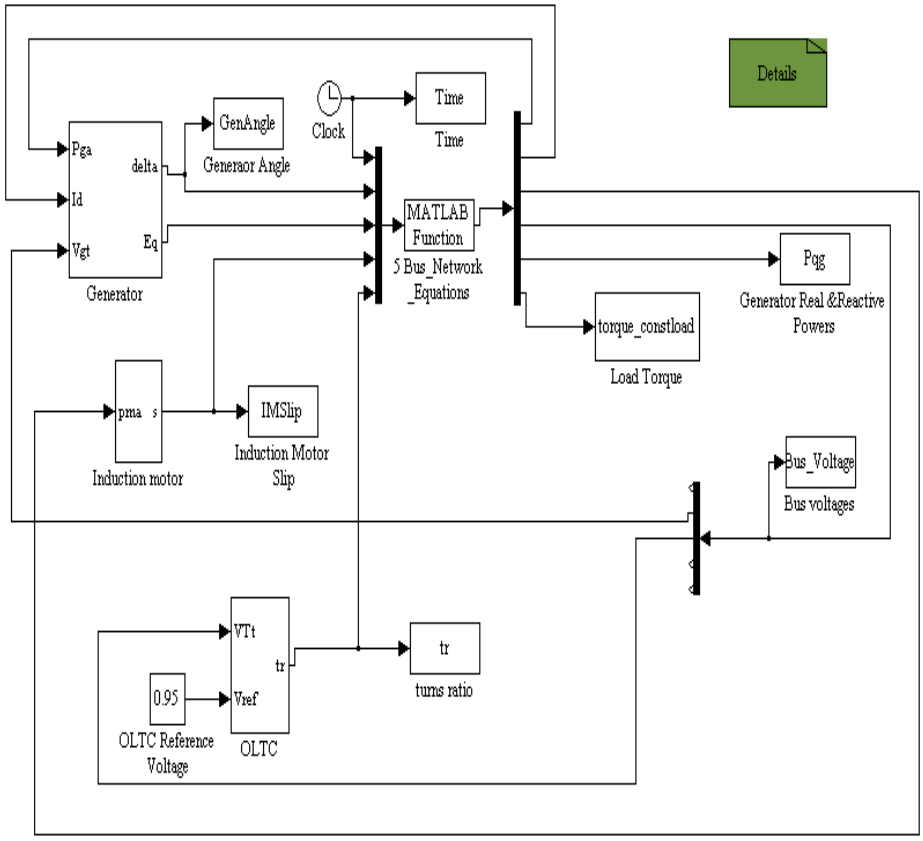

Fig. 3.18 SIMULINK/MATLAB block diagram for long-term voltage stability

3.5 Simulation Results and Discussions

3.5.1 Short-Term Voltage Stability

The short-term voltage stability problem of the system shown in Fig. 3.1 is thoroughly investigated in time domain for two different contingencies (line outage and 3-phase fault). It is considered that the mechanical torque of the aggregated motor remains constant. The data of the system are given in *Appendix A*. The results obtained for the above contingencies are briefly described as follows.

3.5.1.1 System Response due to Sudden Line Outage

Consider that one of the distribution lines connected between buses *A* and *B* in Fig 3.1 is tripped at t = 2.0 secs. Figure 3.19 shows the time response of the motor terminal

voltage V_t (equation (3.2)), internal voltage V_r and the air-gap power P_{ag} (equation (3.5)). At the instant of line outage, the motor power suddenly drops from an initial value of 0.8 pu to 0.705 pu and thus motor start decelerating. The deceleration process increases the slip '*s*' (as per equation 3.4) and that causes to recover the power to the pre-disturbed level. It takes about 2.4 secs to fully recover the power to the original value of 0.8 pu. At line outage, the motor terminal voltage is also suddenly decreased form an initial value of 0.979 pu to 0.905 pu. During the power recovery process, the motor terminal voltage is further decreased to 0.865 pu.

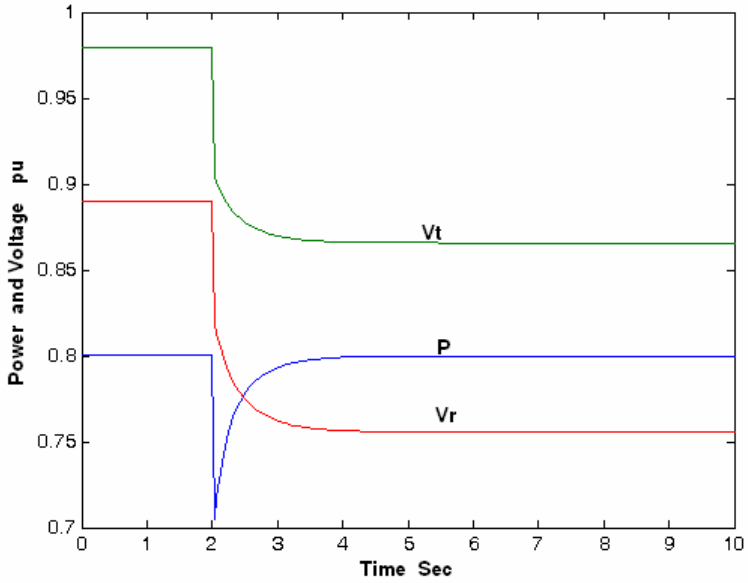

Fig. 3.19 Variation of voltages (V_t, V_r) and load power (P) for a sudden line outage

The variation of voltage against the motor power is shown in Fig. 3.20, where the motor was initially operating at point '*a*' (P_{ag} is 0.8 pu and V_r is 0.89 pu). At line outage, it suddenly jumps to point '*b*' (P_{ag} is 0.705 pu and V_r is 0.82 pu) along the motor *P-V* curve (for a constant slip) and then travel along the path '*b-c*' on post disturbed network *P-V* curve during the power recovery process until it finally reaches the same power at point '*c*' (P_{ag} is 0.8 pu and V_r is 0.755 pu) as explained in section 3.2.2.

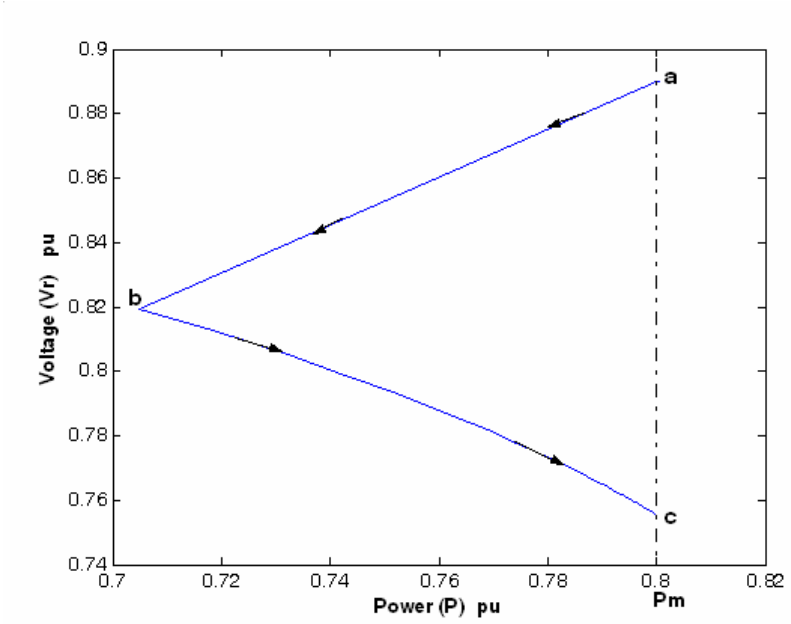

Fig. 3.20 Locus of operation point for single line outage

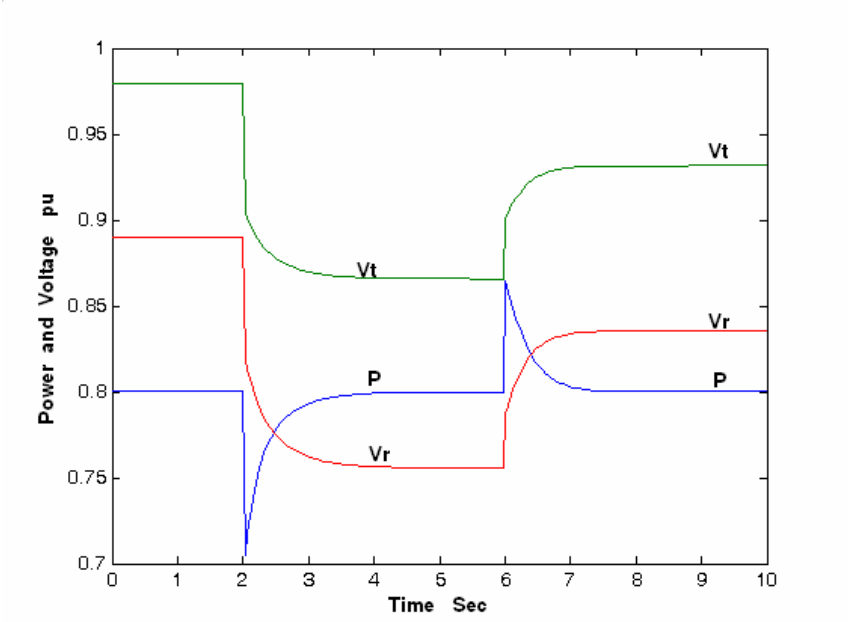

Fig. 3.21 Variation of voltages (V_t, V_r) and load power (P) for a sudden line outage with reactive support at t = 6 sec

It can be observed in Fig. 3.19 that the final motor terminal voltage is 0.865 pu and which may be below the acceptable level. It is thus necessary to improve the terminal voltage of the motor. One way of increasing the terminal voltage is by adding a shunt capacitor at bus B in Fig 3.1. Fig. 3.21 shows the time response of V_t, V_r and P_{ag} for a

sudden line outage at 2 secs followed by switching a shunt capacitor of 0.1875 pu at 6 sec. When the capacitor is added, the voltage as well as power of the motor increased suddenly. Increase of power causes to accelerate the motor (or reduces the slip) until its reaches the same power as the pre-disturbed level. With the capacitor, the motor terminal voltage is now increased to 0.9315 pu.

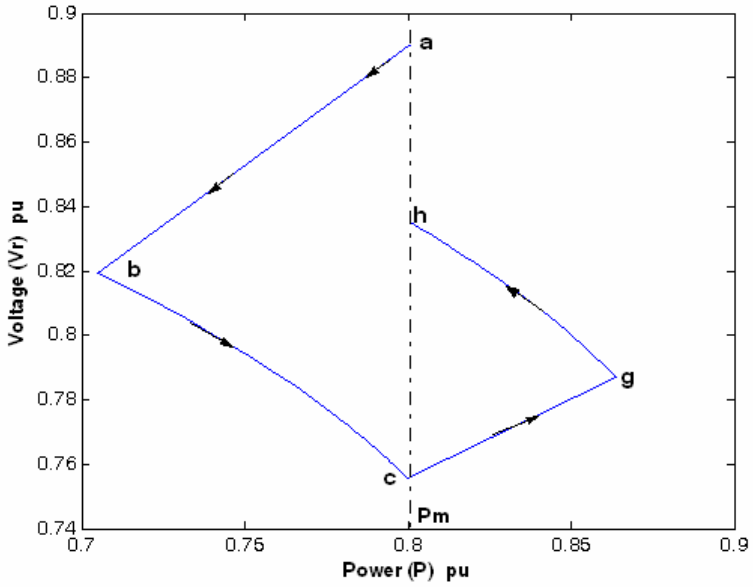

Fig. 3.22 Locus of operation point for single line outage with reactive support at t = 6 sec

The variation of voltage against the motor power is shown in Fig. 3.22. In this case the motor initially is operating at point '*a*' (P_{ag} is 0.8 pu and V_r is 0.89 pu). At line outage, the motor operating point follow the path *a-b-c* as described for Fig 3.20. At capacitor switching, the operating point suddenly jumps from point '*c*' to point '*g*' (P_{ag} is 0.864 pu and V_r is 0.787 pu) along the motor *P-V* curve (at a constant slip) and at point '*g*', the power developed by the motor is more than the load and thus it accelerate and the operating point move to '*h*' (P_{ag} is 0.8 pu and V_r is 0.835 pu) along the network *P-V* curve with capacitor as explained in section 3.2.2 to regain the original power.

3.5.1.2 System Response due to a 3-Phase Fault at Bus A

Now consider that a 3-phase fault (in Fig. 3.1) appears near the motor terminal at 2.0 secs and is cleared by opening one of the lines at 2.15 secs. Fig. 3.23 shows the time

response of V_t, V_r and P_{ag} and it indicates that both the voltage and power of the motor become zero during the faulted period and thus the motor decelerates. However, once the fault is cleared, motor terminal voltage and power suddenly increased to 0.77 pu and 0.835 pu, respectively, and ultimately the motor reaches the pre-disturbed power of 0.8 pu at 5.5 sec. It can also be observed in Fig.3.23 that the motor terminal voltage during post fault period in only 0.865 pu and which is too low. So to improve the voltage a shunt capacitor (0.1875 pu) is added at 6 secs and that helps to increase the voltage to 0.9315 pu as can be seen in Fig. 3.23.

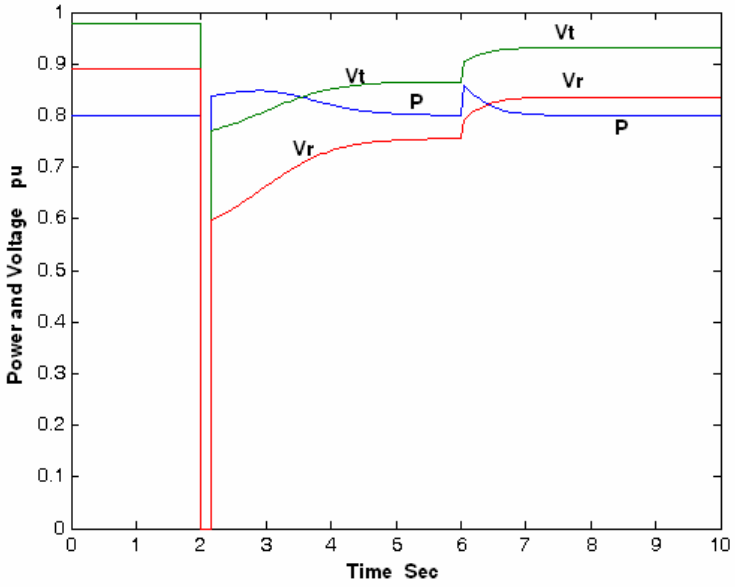

Fig.3.23 Variation of voltages (V_t, V_r) and load power (P) for a 3-phase fault at 2 sec and cleared at 2.15 sec with reactive support at t = 6 sec

The variation of voltage against the motor power for the above case is also shown in Fig. 3.24. In this case the motor is initially operating at point '*d*' (P_{ag} is 0.8 pu and V_r is 0.89 pu). When the fault occurs, the operating point suddenly jumps to zero or origin. When the fault is cleared, the motor operating point moves to point '*j*' (P_{ag} is 0.835 pu and V_r is 0.597 pu) where the power developed by the motor is more than the load. The slip of the motor reduces slowly and the operating point travels along the path '*j-f*' on post fault network *P-V* curve during the power recovery process until it finally reaches the same power at point '*f*' (P_{ag} is 0.8 pu and V_r is 0.755 pu).

At capacitor switching, the operating point suddenly jumps from point '*f*' to point '*g*' (P_{ag} is 0.864 pu and V_r is 0.787 pu) at this point the power developed by the motor is again more than the load, so as per equation (3.4) operating point will move to point '*h*' (P_{ag} is 0.8 pu and V_r is 0.835 pu) along post fault network *P-V* curve with capacitor as explained in Section 3.2.3 to regain the original power.

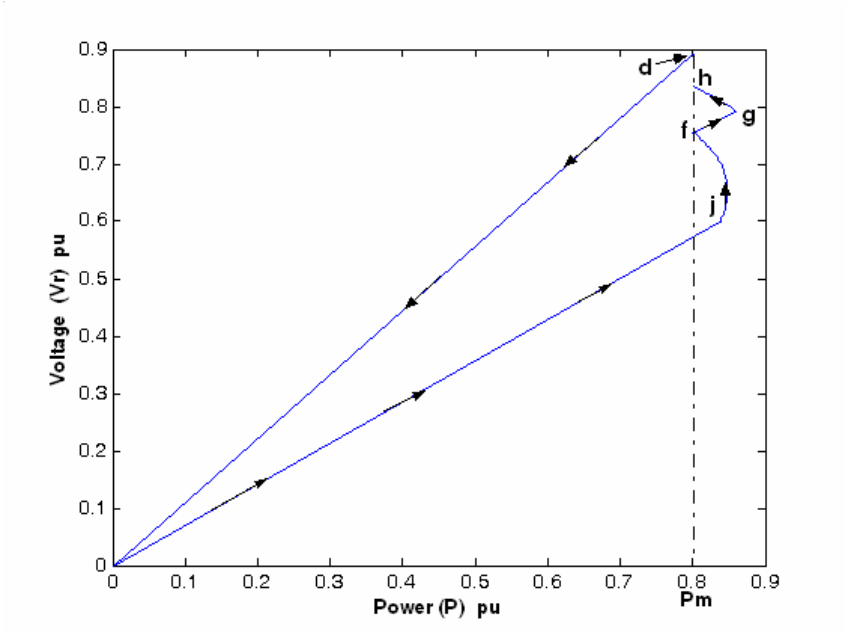

Fig. 3.24 Locus of operation point for a 3-phase fault at 2 sec and cleared at 2.15 sec with reactive support at t = 6 sec

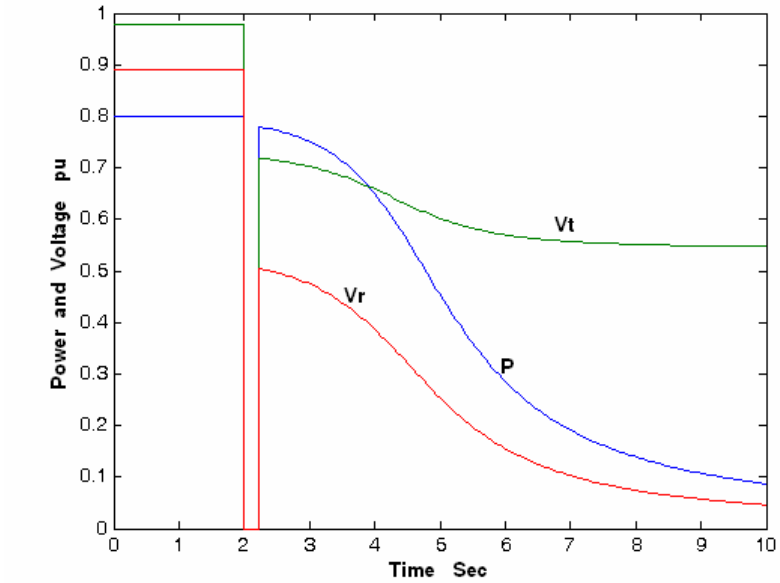

Fig. 3.25 Variation of voltages (V_t, V_r) and load power (P) for a 3-phase fault at 2 sec and cleared at 2.25 sec

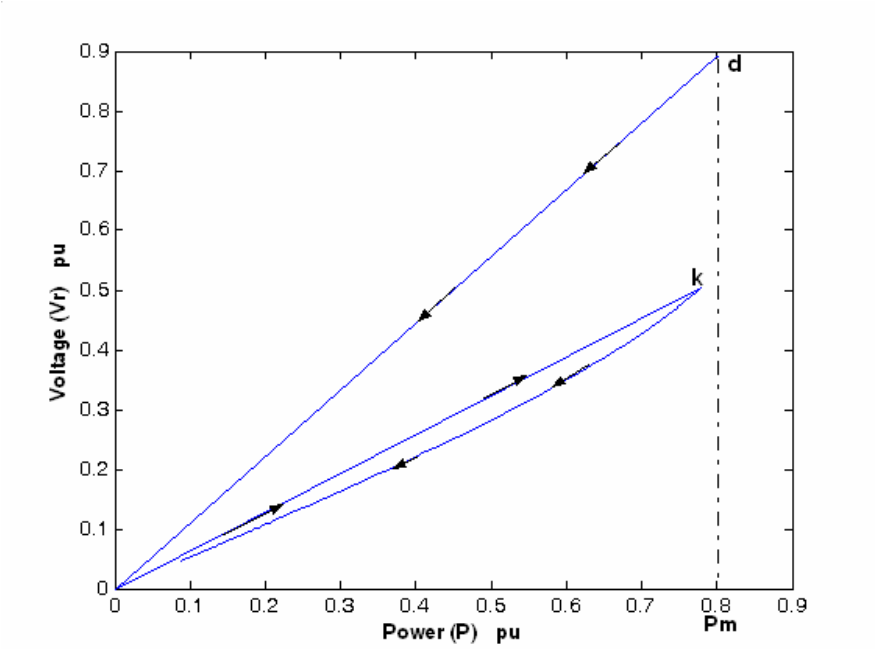

Fig. 3.26 Locus of operation point for a 3-phase fault at 2 sec and cleared at 2.25 sec

As mentioned earlier that if the fault clearing time is delayed, the motor may not reach a stable operating point in post fault period and thus ultimately stall. Fig. 3.25 shows the time response of motor voltage and power when the fault is cleared at 2.25 sec. In this case, the motor power increased to 0.779 pu at fault clearing but which is less than the load power of 0.8 pu. Thus, the motor continues to decelerate in post fault period and eventually stall. The locus of the motor operating point for the above fault case is shown in Fig. 3.26 and it indicates that the motor ultimately approaches the origin.

3.5.1.3 Critical Fault Clearing Time

The torque-slip characteristics of the motor with and without capacitive support (0.3125 pu) at motor terminals are shown in Fig. 3.27 with curve *B* and curve *A* respectively. The maximum torque for cases with and without capacitive support is found as 0.727 pu and 0.603 pu, respectively. Dotted horizontal line in the Fig. 3.27 represents the constant load torque (0.4 pu) on the motor.

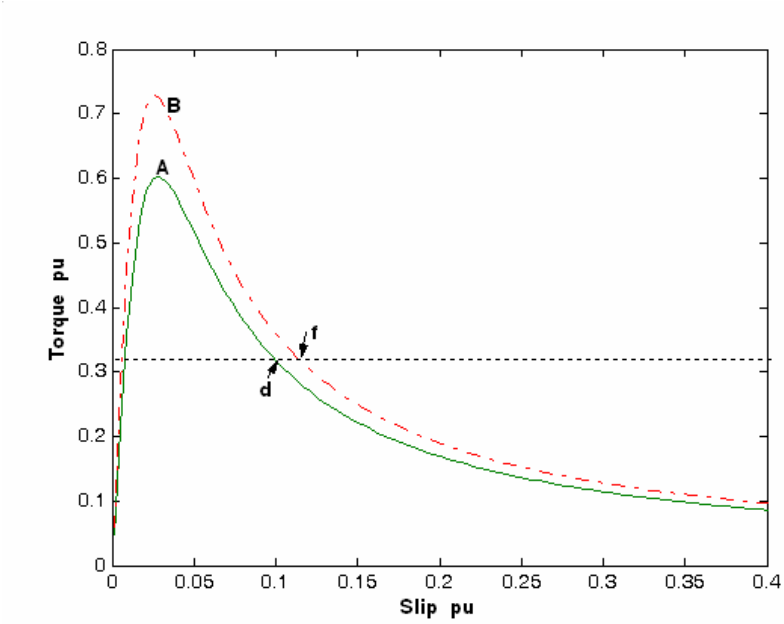

Fig. 3.27 Torque-Slip characteristics of induction motor, A: with single line; B: single line with capacitor at motor terminals

As explained in Sections 3.2.5 and 3.2.6, Tables 3.1 and 3.2 tabulate the t_{cr}, pre-fault stable slip and post-fault unstable slip for various values of load torques. From Table 3.1 it can be observed that for a constant load torque of 0.4 pu the pre fault stable slip, post fault unstable slip and the t_{cr} are 0.0084954 pu, 0.074783 pu and 0.16572 sec respectively. For a stable motor operation at a load torque of 0.4 pu, fault should be cleared before the slip reaches 0.074783 pu (point 'd' in Fig.3.27) Otherwise the motor continues decelerating and increases slip further leading to stalling. From Table 3.1 it can be observed that the post fault unstable slip and t_{cr} for a load torque of 0.65 pu are infeasible because the maximum electrical torque developed by the motor is 0.603 pu (Fig. 3.27) and is less than the mechanical torque (0.65 pu) on the motor. Thus there is no point of intersection of the motor torque-slip characteristic and the load torque T_m and thus the motor would not operate.

Table 3.2 shows the increase in the t_{cr} with capacitive reactive support of 0.3125 pu at the motor terminals. In this case motor was able to operate up to a load torque of 0.727 pu which is greater than that of the without capacitive support case. From Table 3.1 and Table 3.2, it can also be observed that there is an increase in the magnitude of the t_{cr} and post fault unstable slip with the capacitive support.

Table 3.1 Critical fault clearing time (t_{cr})

Load torque (pu)	Pre-fault stable slip (pu)	Post-fault unstable slip (pu)	t_{cr} (Sec)
0.1	0.0019941	0.34441	3.4242
0.2	0.0040451	0.16771	0.81834
0.3	0.0061941	0.10697	0.33592
0.4	0.0084954	0.074783	0.16572
0.5	0.011028	0.053097	0.084138
0.6	0.013924	0.031102	0.02863
0.65	0.0156	0.0258 - 0.0106i	0.0158 - 0.0162i

Table 3.2 Critical fault clearing time (t_{cr}) with capacitive support

Load torque (pu)	Pre-fault stable slip (pu)	Post-fault unstable slip (pu)	t_{cr} (Sec)
0.1	0.0017415	0.3851	3.8335
0.2	0.003524	0.18907	0.92772
0.3	0.0053756	0.1224	0.39008
0.4	0.0073312	0.087881	0.20137
0.5	0.0094387	0.065923	0.11297
0.6	0.011769	0.049649	0.063133
0.7	0.014442	0.034465	0.028605
0.75	0.0160	0.0251 - 0.0063i	0.0122 - 0.0084i

Fig. 3.28 and Fig. 3.29 show the variation in the slip with time for the cases of without and with capacitive support respectively. From Table 3.1 it can be observed that the t_{cr} for a load torque of 0.4 pu is the 0.16572 sec. Consider the fault appear at t =1.0 sec. When the fault is cleared within 1.16572 sec, motor slip initially increases slightly and then decreases to normal stable value as can be seen in Fig 3.28 (solid line). When the fault is cleared after 1.16572 sec (i.e. 1.7 sec), motor slip increases monotonically and ultimately stall the motor as can be seen in Fig 3.28 (dashed line). With the additional fixed capacitive support (0.3125 pu) at motor terminals, the value of t_{cr} for the same load torque (0.4 pu) is increased from 0.16572 sec to 0.20137 sec (see Table 3.1 and Table 3.2). The same can be confirmed from the result shown in

Fig 3.29. In Fig. 3.29 the solid and dashed lines show the variation of slip with the fault clearing time of 1.201 sec and 1.21 sec, respectively.

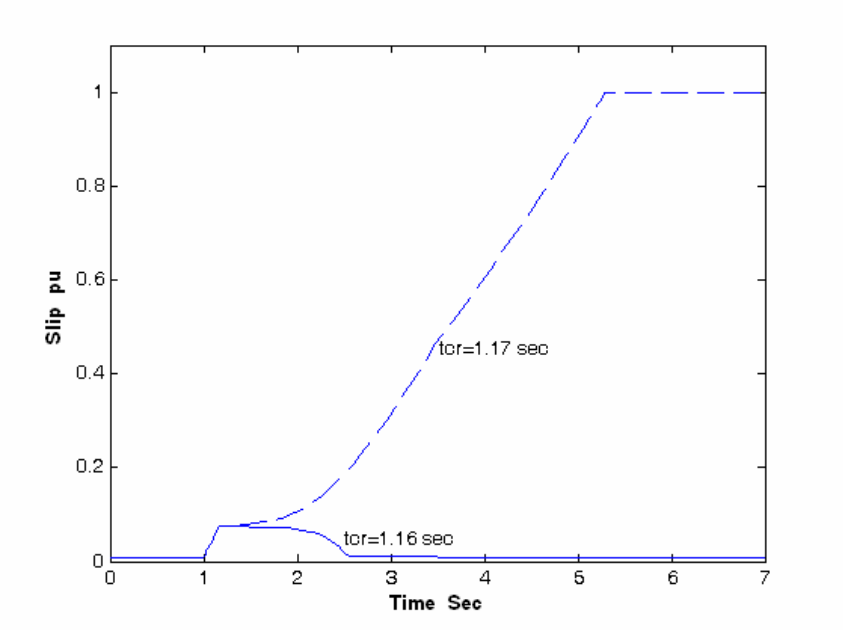

Fig. 3.28 Variation of the slip with time

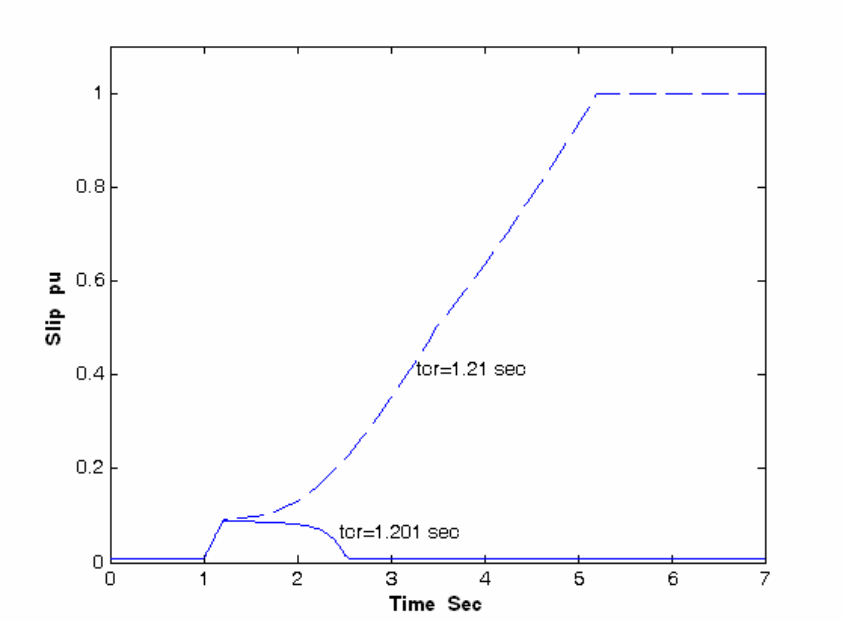

Fig. 3.29 Variation of the slip with time with capacitive support

3.5.2 Long-Term Voltage Stability

The long-term voltage stability of the system of Fig. 3.10 is thoroughly studied for various load levels of the induction motor. The data of the system is given in Appendix A. Three different load conditions, as given in Table 3.3, are considered. In all cases, the long-term dynamic voltage stability of the system is evaluated by assuming that one of the parallel transmission lines connected between buses 1 and 4 is suddenly tripped at 300 seconds. The results obtained for the above cases are briefly described in the following.

Table 3.3 Different load conditions of the induction motor

	Coefficients of load torque		
	T_c (pu)	T_s (pu)	T_q (pu)
Case 1	0.3	0.1	0.1
Case 2	0.6	0.1	0.1
Case 3	0.65	0.1	0.1

First, the dynamics of the system are evaluated for the light load condition (case 1). Fig. 3.30 shows the variation of load bus voltage (V_3) and turns ratio (t_r) of the OLTC transformer and it indicates that when t_r = 1.0 pu, the load bus voltage is at 0.906 pu, which is less than the reference voltage (0.95 pu). So OLTC starts operation after an initial delay of 30 secs and decreases successively until the load voltage reached the desired value of 0.95 pu (within the dead band of 0.015 pu). It takes about 90 secs to reach the steady state condition. When the line tripped at 300 secs, the load voltage momentarily decreases and then the OLTC transformer again starts changing its turns ratio in steps with an initial delay of 30 secs and subsequent delays of 10 secs. In this case, the system is capable of restoring the load voltage to the pre-disturbed level of 0.95 pu by using the OLTC transformer and the local generator without reaching their limiting values. Fig 3.31 shows the variation of the field current of the generator. The initial field current of the generator is 2.145 pu. When the line tripped at 300 secs, field current suddenly increased to 2.45 pu, which is within the limiting value of 2.825 pu, to support the voltage by increasing the reactive power supply by the generator.

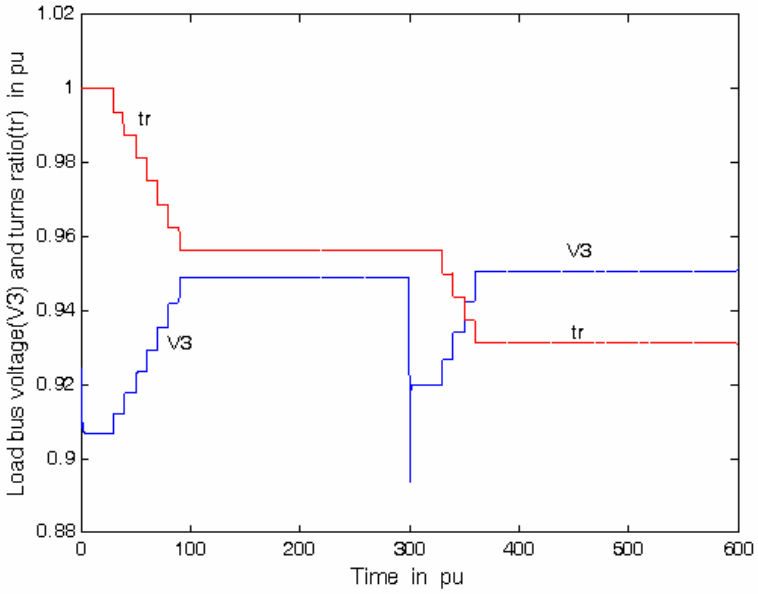

Fig. 3.30 Variation of load bus voltage and OLTC turns ratio for case 1

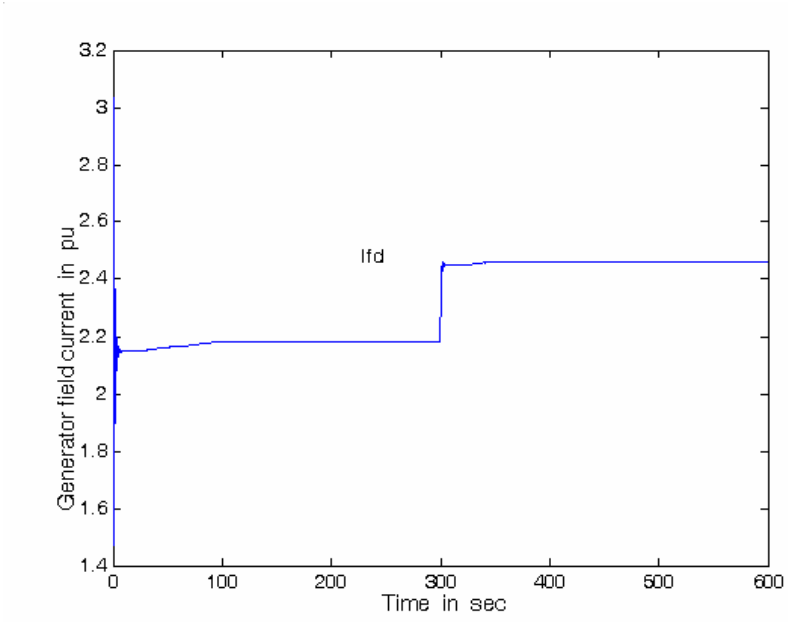

Fig.3.31 Variation of generator field current for load case 1

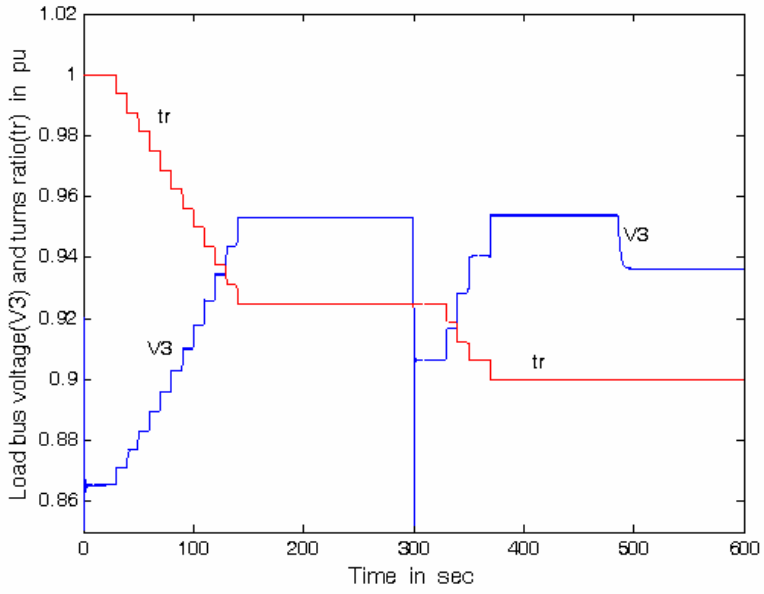

Fig. 3.32 Variation of load bus voltage and OLTC turns ratio for case 2

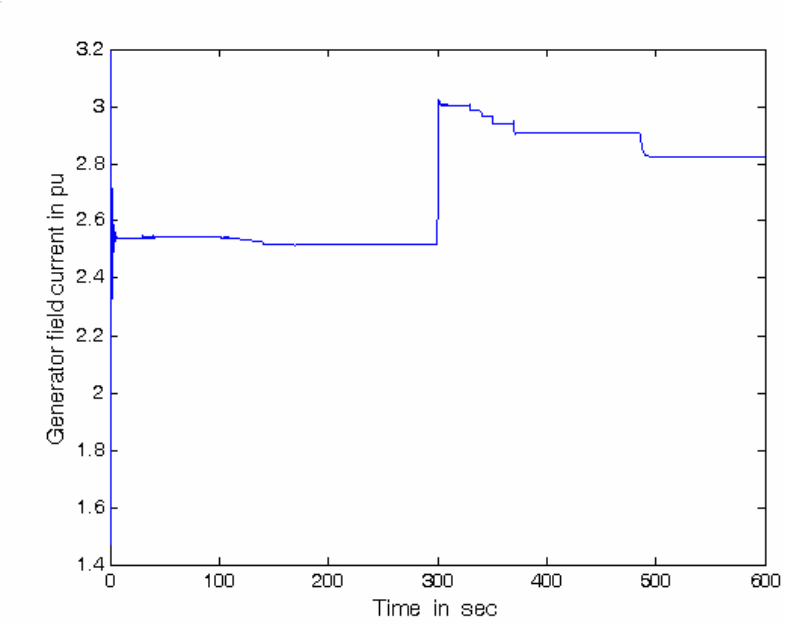

Fig.3.33 Variation of generator field current for load case 2

When the constant component of load torque of the induction motor is increased to 0.6 pu (case 2), the initial values of t_r and V_3 are found as 1 pu and 0.8655 pu respectively, In this case, V_3 is less than V_{ref}. So OLTC starts its operation and increases the load voltage to desired value of 0.95 pu. It takes about 140 secs to reach the steady state condition. When the line tripped at 300 secs, the load voltage suddenly decreases to 0.905 pu and thus the OLTC transformer again starts changing

its turns ratio in steps. The combined afford of OLTC and local generator can restore the load voltage to the pre-disturbed level of 0.95 pu at about 370 secs (see Fig. 3.32). Fig. 3.33 shows the variation of generator field current and it indicates that the field current before the disturbance was 2.52 pu, and at line outage it suddenly jumps to 3 pu then reduces slowly in steps to 2.91 pu at 370 sec. In post-disturbed period the field current of the generator exceeded the limit of 2.825 pu and that causes the activation of the OXL at 485.5 secs. When the OXL is activated, the field current of the generator reduces to the limiting value of 2.825 pu. Reduction of field current causes the reduction of reactive power supplied by the generator, which cause the reduction in the load voltage to 0.9365 pu. However, there are no more remaining taps of the OLTC to improve the load voltage further. Even though the actual load voltage is slightly lower than the desired value, the motor is capable of delivering the required torque without stalling. In this case, the system can be considered as stable in both short-term and long-term but unable to maintain the desired load voltage.

Fig 3.34 shows the variation of V_3 and t_r for the increased load condition (case 3). In this case, the initial load bus voltage was at 0.853 pu, and thus the OLTC started its operation as mentioned in the earlier case and improved the load voltage to the desired value of 0.95 pu in about 150 sec. When the line tripped at 300 secs, the load voltage suddenly dropped to 0.9 pu, so again the OLTC transformer started its operation to improved the load voltage to 0.95 pu. But in this case, most of the OLTC steps have already been utilized to improve the voltage, so only a few steps are left to increase the voltage further. At 350 sec the OLTC reached its minimum steps limit and therefore the load bus voltage cannot be improved further even though it is less than the OLTC reference voltage (0.95 pu).

Fig. 3.35 shows the variation of generator field current and it indicates that the field current suddenly jumped to 3.15 pu at line outage and then it reduces slowly to 3.09 pu at 340 secs. In post-disturbed period, the field current of the generator exceeds the limiting value of 2.825 pu for a prolong period (see Fig. 3.35) and that caused to active the OXL at 369.5 secs. When the OXL is activated, the field current of the generator temporarily reduces to the limiting value of 2.825 pu. Reduction of field current decreases the load voltage significantly and that caused to stall the motor almost immediately at 369.5 secs. Stalling the motor initiates the voltage collapse

process as can be seen in Fig. 3.35. In this case, the system can be considered as short-term stable because it survived for the first 69.5 secs following the disturbance. However, the system is long-term unstable because the voltage collapsed after 69.5 secs of the disturbance.

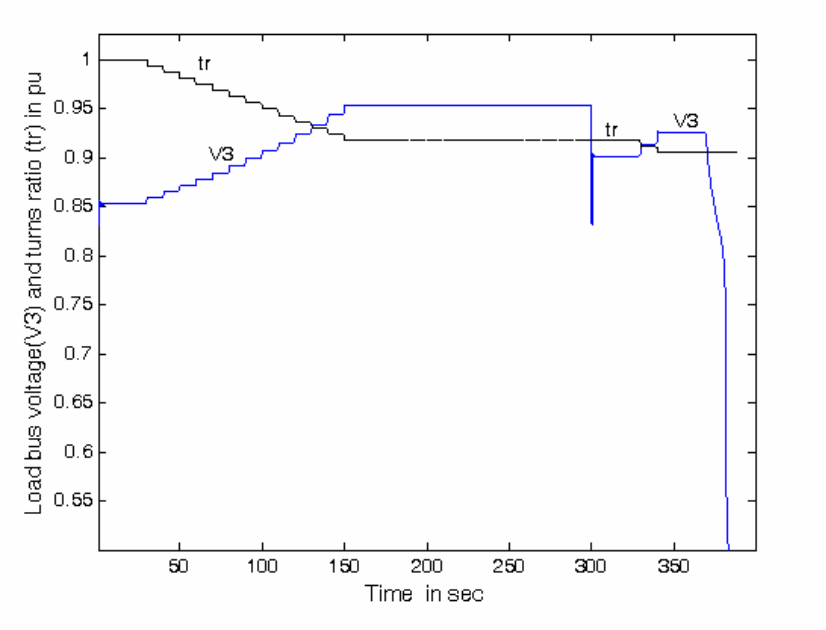

Fig. 3.34 Variation of load bus voltage and OLTC turns ratio for case 3

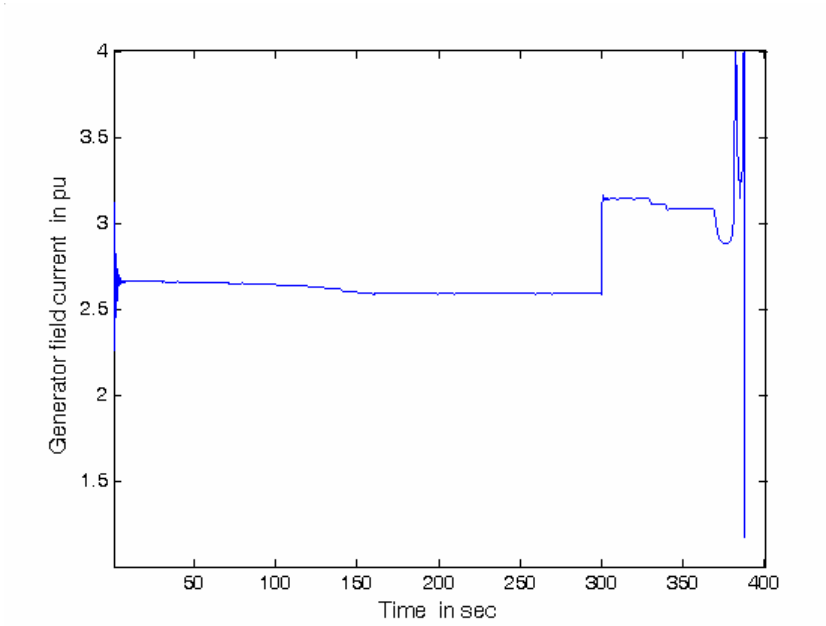

Fig. 3.35 Variation of generator field current for load case 3

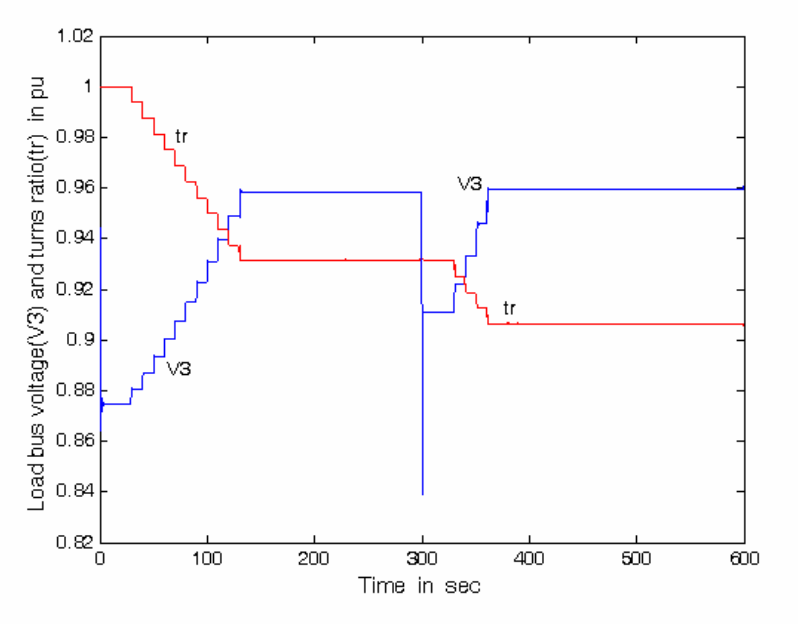

Fig. 3.36 Variation of load bus voltage and OLTC turns ratio for case 3 with a fixed capacitor of 0.125 pu at bus 3

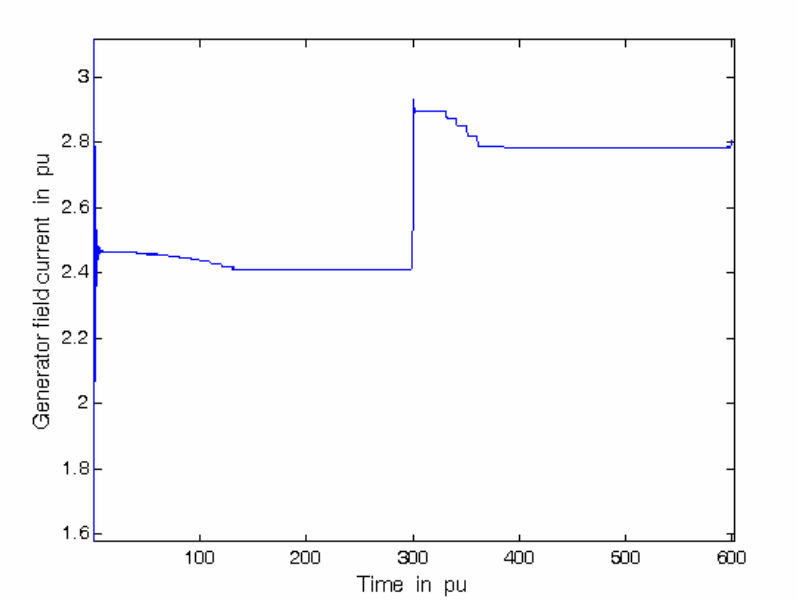

Fig. 3.37 Variation of generator field current for load case 3 with a fixed capacitor of 0.125 pu at bus 3

One way of preventing the long-term voltage collapse is to increase the load voltage level by providing adequate reactive power support from other sources. Fig. 3.36 shows that the variation of load voltage and turns ratio of the OLTC transformer when

a shunt capacitor of 0.125 pu is placed at bus 3. It can be observed from Fig. 3.36 that the system is stable for both short-term and long-term, and capable of restoring the desired load voltage of 0.95 pu following the disturbance. The variation of field current of the generator is shown in Fig. 3.37. It indicates that, following the disturbance, the field current exceeds the limit for a short period of time and is not adequate to activate the OXL. The field current ultimately reduces to 2.785 pu (below the limiting value) at 360 sec and that prevents activation of the OXL.

3.6 Summary

Models of various power system components (such as OLTC, OXL, AVR, generators, induction motors, exponential load models etc.,) were successfully developed using SIMULINK and MATLAB. The effect of induction motor load on short-term voltage stability of a simple power system was investigated. These results, obtained using the *P-V* curves, were verified through the time domain simulation results.

Effects of the dynamics of slow-acting devices, such as transformer with OLTC, generators with OXL, etc., were investigated for long-term voltage stability of a power system. The above investigation improved the understanding about the reasons of voltage collapse and that helped to take remedial action in preventing the voltage collapse by providing adequate reactive power support.

Chapter 4

Determination of Static Voltage Stability Index

4.1 Introduction

Voltage collapse occurs typically when a system is subjected to heavy loading, sudden unexpected disturbances (line outages and/or faults) and reactive power shortages. Although many variables involved, in general, voltage instability is associated with the reactive power demands of the loads not being met because of limitations on generation and transmission of reactive power. Out of the two approaches (static and dynamic), the dynamic approach of voltage collapse has been demonstrated in Chapter 3.

In this chapter, the static approach of voltage collapse is considered. Here steady state model of system components is used to analyze the voltage collapse problem. Static approach is mainly important in the planning stage. Many methods based on system's Jacobian were reported in the literature. Jacobian based methods utilize either sensitivity or eigenvalue behavior of the Jacobian matrix to determine its closeness to singularity. These methods are computational intensive and time consuming [3].

However there are some methods based on local phasors were reported in the literature [12, 46-48] and they suggest that the local quantities (voltage and current phasors) contain enough information to identify the areas which are prone to voltage collapse [12]. These aspects provided enough motivation to the author to suggest a method that is computationally less intensive and provides more information to the system operator.

In general, voltage instability is associated with the shortage of reactive power support to maintain adequate voltage profile. Thus, identification of the weakest segment of a large power network in the planning stage is very important for appropriate reactive power compensation to avoid voltage collapse [1-3].

In this chapter, a new method to estimate the static voltage stability index of a power system based on the complex voltage information of all buses in the system is proposed. The method mainly focuses on the identification of critical power flow path and more specifically identification of critical bus and critical line in a power system.

4.2 Proposed Methodology

The proposed methodology aims at developing a procedure to determine the voltage stability index (*VSI*) of a general power system. Initially an expression for line voltage stability index (*LVSI*) in a simple two-bus system is derived. This expression is then updated to include the effect of an off-nominal tap setting transformer. For the case of a general power system, *LVSI* of all lines are determined using bus voltage magnitudes and angle generated by the load flow program. Possible power flow paths are then identified based on the *LVSI* values of the lines. This is followed by determining an index for each power flow path, and is called power flow path voltage stability index (*PVSI*). The power flow path with minimum *PVSI* is considered as the critical power flow path of the system. The *PVSI* of the critical power flow path is then considered as the *VSI* of the overall power system. The critical line and critical bus are then identified based on the *LVSI* values of the lines in the critical power flow path.

4.2.1 Determination of *LVSI*

4.2.1.1 Two-Bus System

Consider a simple two-bus system where the source bus '*i*' is connected to the load bus '*j*' through a transmission line having an impedance of $\mathbf{Z}_{\text{line}}$ as shown in Fig 4.1. The current through the line as well as through the load impedance ($\mathbf{Z}_l$) is considered as **I**. The complex voltage at buses '*i*' and '*j*' is considered as $V_i \angle \delta_i$ and $V_j \angle \delta_j$, respectively.

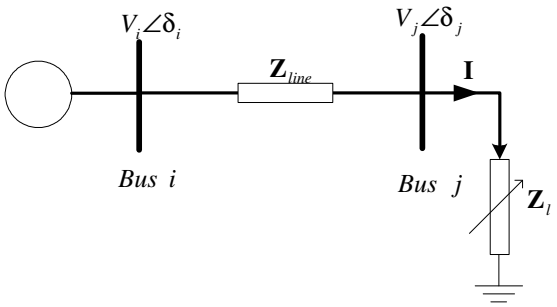

Fig. 4.1 Simple two bus system to determine *LVSI*

According to the maximum power transfer theorem, when the magnitude of load impedance (Z_l) becomes the same as the magnitude of the line impedance (Z_{line}), the system reaches the maximum power point or the critical point at which the voltage collapse occurs. Thus at voltage collapse point

$$Z_{line} = Z_l \tag{4.1}$$

Under normal load conditions, the magnitude of voltage drop across the transmission line is less than the magnitude of load bus voltage. When the system reaches its maximum power transfer level, the magnitude of voltage drop across the transmission line becomes the same as the magnitude of load bus voltage. Therefore within the voltage stability limit, the relationship between the load voltage and voltage drop can be written as

$$\left|\mathbf{V}_i - \mathbf{V}_j\right| \le \left|\mathbf{V}_j\right| \tag{4.2}$$

Equation (4.2) is in the form of complex variables and can be simplified to magnitude form as

$$V_i^2 + V_j^2 - 2V_iV_jCos\left(\delta_i - \delta_j\right) \le V_j^2 \tag{4.3}$$

After bringing the right hand side term to left hand side, the above equation can be written as

$$V_i^2 - 2V_iV_jCos\left(\delta_i - \delta_j\right) \le 0 \tag{4.4}$$

Divide both sides of the above equation by V_i^2

$$2\frac{V_j}{V_i}Cos\left(\delta_i - \delta_j\right) - 1 \ge 0 \tag{4.5}$$

At no load condition, $V_i = V_j$ and angle $\delta_i = \delta_j$ and thus the left hand side (*LHS*) of equation (4.5) becomes unity. Under normal operation (between no load and the maximum load) *LHS* of equation (4.5) will be greater than zero but less than unity. At

the maximum loading condition (voltage collapse) the equality sign hold and it becomes zero. From the above reasoning, the voltage stability index of the line at bus '*j*' ($LVSI_j$) can be expressed as follows

$$LVSI_j = 2\frac{V_j}{V_i}Cos(\delta_i - \delta_j) - 1 \tag{4.6}$$

Similarly *LVSI* at bus '*i*' can be expressed as

$$LVSI_i = 2\frac{V_i}{V_j}Cos(\delta_j - \delta_i) - 1 \tag{4.7}$$

The magnitude of $LVSI_j$ and $LVSI_i$ depends on the direction as well as amount of power flow.

The voltage collapse proximity index described in [12] is similar to the expression (4.6). In [12], the singularity condition of the Jacobian matrix is used to determine the voltage collapse criterion. In the present work, the maximum power transfer theorem is used in determining the voltage stability index.

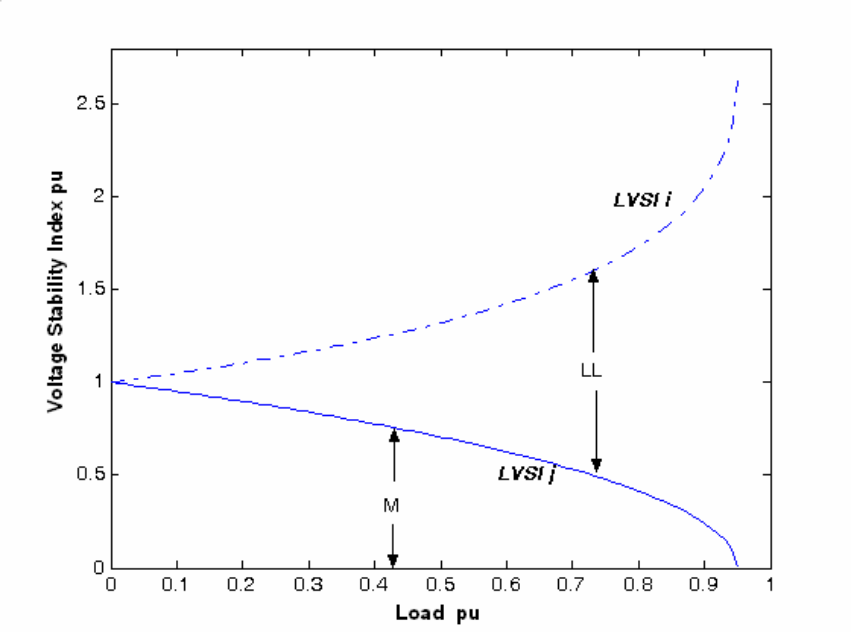

Fig. 4.2 Variation of $LVSI_j$ and $LVSI_i$ with system load

Typical variations of $LVSI_j$ and $LVSI_i$ against the system load are shown in Fig 4.2 and is plotted for V_i = 1.0 pu and $\mathbf{Z_{line}}$ = 0.0897 + 0.2752j pu. Fig. 4.2 indicates that at no load, both $LVSI_j$ and $LVSI_i$ have the same value (unity) because $V_i = V_j$ and $\delta_i = \delta_j$. As the load increases, $LVSI_j$ decreases and reaches zero value at voltage collapse point. While $LVSI_i$ increases and in the present case it reaches a value of 2.6335 pu at voltage collapse point. In Fig 4.2 the value of $LVSI_j$ can be interpreted as voltage stability index (M in Fig. 4.2). M varies in between one (at no load) and zero (at voltage collapse point). At the same time the difference between $LVSI_j$ and $LVSI_i$ ('*LL*' in Fig. 4.2) can be considered as a measure of line loading. At no load, '*LL*' is zero ($LVSI_j = LVSI_i$) and it increases with load.

4.2.1.2 Two-Bus System with a Off-Nominal Tap Setting Transformer

Consider an off-nominal tap setting transformer with an impedance of ($\mathbf{Z_T}$) is connected between bus '*i*' (source bus) and bus '*j*' (load bus) as shown in Fig. 4.3. The equivalent π circuit model of the transformer is shown in the Fig. 4.4, where $\mathbf{Z}_{ij}$, $\mathbf{Z}_{ij1}$ and $\mathbf{Z}_{ij2}$ are equivalent mutual impedance, shunt impedance on side '*i*' and side '*j*' respectively. If the off-nominal turns ratio of the transformer is a: 1, $\mathbf{Z}_{ij}$, $\mathbf{Z}_{ij1}$ and $\mathbf{Z}_{ij2}$ are given by [52]

$$\mathbf{Z}_{ij} = (a)\mathbf{Z}_T \tag{4.8}$$

$$\mathbf{Z}_{ij1} = \left(\frac{a^2}{1-a}\right)\mathbf{Z}_T \tag{4.9}$$

$$\mathbf{Z}_{ij2} = \left(\frac{a}{a-1}\right)\mathbf{Z}_T \tag{4.10}$$

If off-nominal turns ratio of the transformer is 1: a, $\mathbf{Z}_{ij}$, $\mathbf{Z}_{ij1}$ and $\mathbf{Z}_{ij2}$ are given by [51]

$$\mathbf{Z}_{ij} = (a)\mathbf{Z}_T \tag{4.11}$$

$$\mathbf{Z}_{ij1} = \left(\frac{a}{a-1}\right)\mathbf{Z}_T \tag{4.12}$$

$$\mathbf{Z}_{ij2} = \left(\frac{a^2}{1-a}\right)\mathbf{Z}_T \tag{4.13}$$

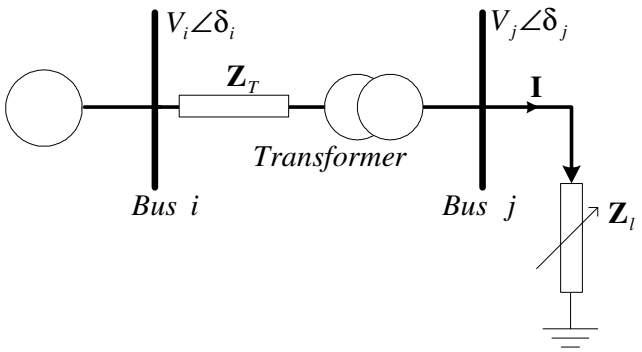

Fig. 4.3 Simple two-bus system with transformer having off nominal turns ratios

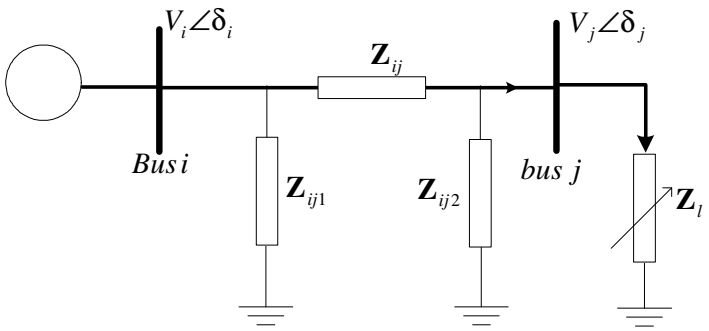

Fig. 4.4 Equivalent circuit of Fig 4.3

Replace the generator and the transformer by Thevenin equivalent circuit. When the source at bus '*i*' is considered as ideal i.e. constant voltage with zero source impedance, the parameters of the Thevenin equivalent circuit (Z_{th}, V_{th} and δ_{th}) with an off nominal transformer with turns ratio a: 1 are given by

$$\mathbf{Z}_{th} = \mathbf{Z}_{ij} \| \mathbf{Z}_{ij2} = \frac{\mathbf{Z}_{ij}\,\mathbf{Z}_{ij2}}{\mathbf{Z}_{ij} + \mathbf{Z}_{ij2}} \tag{4.14}$$

$$V_{th} = \frac{\mathbf{V}_i}{\mathbf{Z}_{ij} + \mathbf{Z}_{ij2}}\mathbf{Z}_{ij2} = \frac{V_i}{a} \tag{4.15}$$

When the effect of transformer resistance is neglected, the angle δ_{th} will be the same as δ_i

$$\delta_{th} = \delta_i \tag{4.16}$$

Similarly for transformers with 1:a off-nominal turns ratio, the expressions for Z_{th} and δ_{th} remain the same but V_{th} is given by

$$V_{th} = \frac{\mathbf{V}_i}{\mathbf{Z}_{ij} + \mathbf{Z}_{ij2}} \mathbf{Z}_{ij2} = aV_i \tag{4.17}$$

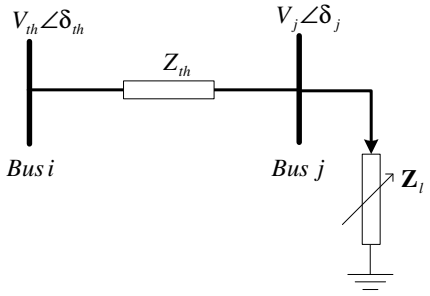

Fig. 4.5 Equivalent circuit of Fig 4.4

The Thevenin equivalent circuit of the system (Fig 4.4) is shown in Fig 4.5 and it is similar to Fig 4.2. Thus $LVSI_j$ and $LVSI_i$ of Fig 4.5 can be evaluated from equations (4.6) and (4.7) respectively by replacing V_i by aV_i (for 1:a off-nominal turns ratio) or V_i/a (for a:1 off-nominal turns ratio)

4.2.1.3 *LVSI* of a Transmission Line in a General Power System

Evaluation of the proposed line voltage stability index through equations (4.6) and (4.7) requires only the complex bus voltages and it does not require the generator, load and line parameters. Such a simple requirement can fully be exploited to evaluate the voltage stability index of a transmission line in a general power system as shown in Fig. 4.6. It requires only the complex voltages at buses '*i*' and '*j*' (at both ends of the line). For the transmission line (between buses '*i*' and '*j*') shown in Fig 4.6, *LVSI*

at bus '*j*' side and *LVSI* at bus '*i*' side can again be determined using the expressions (4.6) and (4.7) respectively.

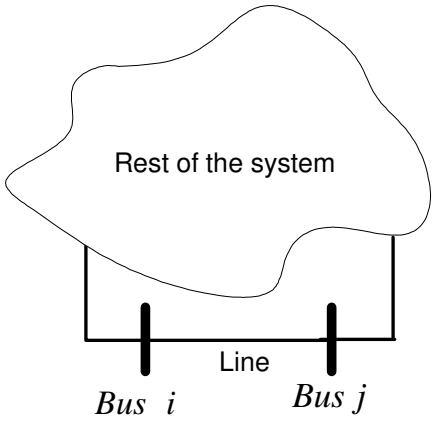

Fig. 4.6 Transmission line connected between buses '*i*' and '*j*' in a general power system

4.2.2 Determination of *VSI* of a General Power System

In general, power system networks are of mesh type and thus it is important to determine the *VSI* of a mesh network. First compute the *LVSI* at both ends of all branches (lines and transformers) of the network using the load flow results. In a branch, power flows from higher *LVSI* to lower *LVSI*. Higher *LVSI* side can be considered as stronger side (or upstream side) while the lower *LVSI* side can be considered as weaker side (downstream side). Based on the $LVSI_j$ and $LVSI_i$, the mesh network is then decomposed into a number of power flow paths.

Identification of power flow path starts at a source bus (or upstream side) and proceed to all downstream side buses which are connected through a branch to the upstream side bus provided the *LVSI* of the branch at upstream side has higher value than that at the downstream side. If the branch has lower *LVSI* at the upstream side than that at the downstream side, it should not be considered in the path. The above process is to be continued until it is found that no additional branch can be added to the path because of having lower *LVSI* at the upstream side compared to the downstream side.

For example, consider the IEEE 30 bus test system as shown in Fig. 4.7. The data of the system are obtained from [53-54] and given in Appendix A. In this system there are five *PV* buses (buses 2, 5, 8, 11, 13) and twenty-four *PQ* buses, Bus no 1 is chosen as slack bus. Voltage magnitudes and angles of all the buses of test system at base load condition are given in Table 4.1. Using the results of the base case load flow (Table 4.1), the *LVSI* at both ends of all branches are computed through equations (4.6) and (4.7) and the values found are also shown in Fig 4.7.

Table 4.1 IEEE 30 bus system bus voltage magnitude and angle at base load

Bus no	Voltage Magnitude pu	Angle degree
1	1.060	0
2	1.043	-5.497
3	1.022	-8.004
4	1.013	-9.6615
5	1.010	-14.381
6	1.012	-11.398
7	1.003	-13.150
8	1.010	-12.115
9	1.051	-14.434
10	1.044	-16.024
11	1.082	-14.434
12	1.057	-15.302
13	1.071	-15.302
14	1.042	-16.191
15	1.038	-16.278
16	1.045	-15.880
17	1.039	-16.188
18	1.028	-16.884
19	1.025	-17.052
20	1.029	-16.852
21	1.032	-16.468
22	1.033	-16.455
23	1.027	-16.662
24	1.022	-16.830
25	1.018	-16.424
26	1.001	-16.842
27	1.026	-15.912
28	1.011	-12.057
29	1.006	-17.136
30	0.994	-18.015

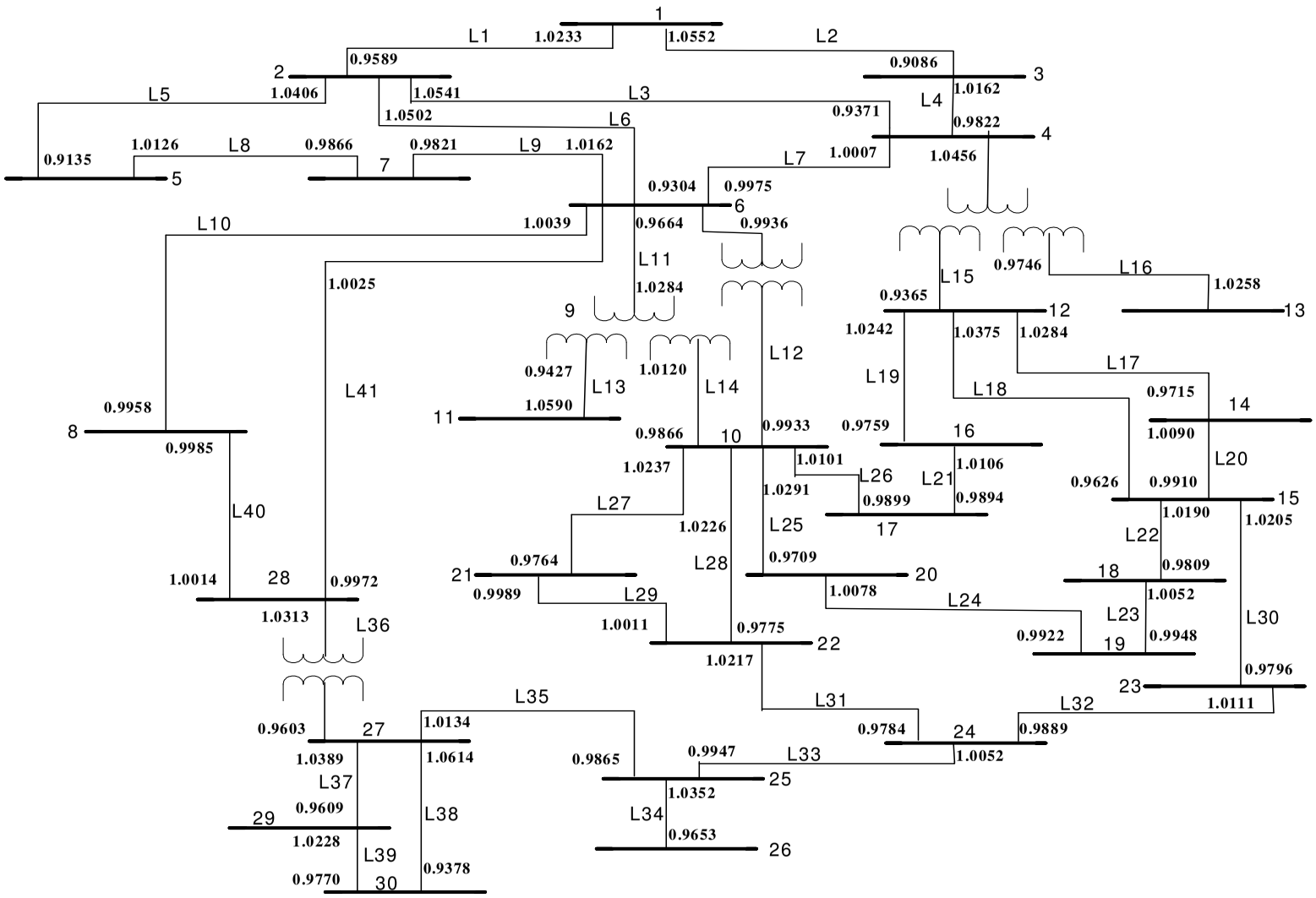

Fig. 4.7 IEEE 30-bus test system

Let us start the identification of power flow paths at source bus 1, which is connected to bus 2 and bus 3 via lines L_1 and L_2 respectively. Line L_1 has a *LVSI* of 1.0233 (near bus 1) and 0.9589 (near bus 2). Since *LVSI* in the upstream side (bus 1) is higher than that at the downstream side (bus 2), the line should be included in the path. Similarly line L_2 should also be included in the path. Now start at bus 2, which is connected to buses 4, 5 and 6 through lines L_3, L_5 and L_6 respectively. Again all the lines have higher *LVSI* at the upstream side compared to the downstream side and thus they should be included in the path. Bus 5 is connected to bus 7 through line L_8, which has a *LVSI* of 1.0126 (near bus 5) and 0.9866 (near bus 7). Since *LVSI* in the upstream side (bus 5) is higher than that at the downstream side (bus 7), the line should be included in the path. Now bus 7 is connected to bus 6 through line L_9 that has lower *LVSI* (0.9821) at the upstream side (bus 7) compared to the downstream side (1.0162 at bus 6) and thus it should not be considered in the path. In this case the path terminates at bus 7 as shown in Fig. 4.8. The above technique is to be repeated to identify the other possible power flow paths of the system. All power flow paths that start at bus 1 are given in Table 4.2.

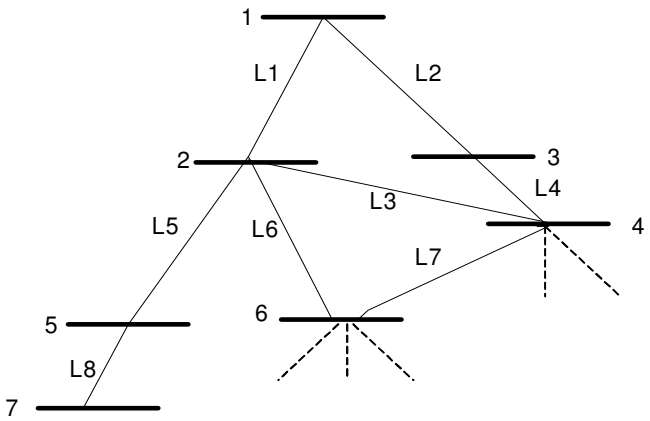

Fig. 4.8 Power flow path identification

After identifying the all-possible power flow paths, it is required to calculate the *PVSI* of each power flow path. In the present study, the *PVSI* is assumed as the cumulative product of $LVSI_j$ of all lines that constitute the path. Therefore *PVSI* can be written as

$$PVSI = \prod_{k \in \zeta} LVSI_{kj} \tag{4.18}$$

where ζ is a set of lines that constitute a power flow path and 'j' is the downstream side of the line.

Table 4.2 Power flow paths starting from bus 1 at based load

Path no	Bus numbers in the power flow path								
P_1	1	2	4	6	7				
P_2	1	2	4	6	8				
P_3	1	2	4	6	10	17			
P_4	1	2	4	6	10	20			
P_5	1	2	4	6	10	20	19		
P_6	1	2	4	6	10	21			
P_7	1	2	4	6	10	22	21		
P_8	1	2	4	6	10	22	24		
P_9	1	2	4	6	10	22	24	25	26
P_{10}	1	2	4	6	28	8			
P_{11}	1	2	4	6	28	27	25	26	
P_{12}	1	2	4	6	28	27	29	30	
P_{13}	1	2	4	6	28	27	30		
P_{14}	1	2	4	12	16	17			
P_{15}	1	2	5	7					
P_{16}	1	2	6	7					
P_{17}	1	2	6	10	17				
P_{18}	1	2	6	10	20	19			
P_{19}	1	2	6	10	22	21			
P_{20}	1	2	6	28	8				
P_{21}	1	2	6	28	27	25	26		
P_{22}	1	2	6	28	27	29	30		
P_{23}	1	2	6	28	27	30			
P_{24}	1	3	4	6	7				
P_{25}	1	3	4	6	8				
P_{26}	1	3	4	6	10	17			
P_{27}	1	3	4	6	10	20	19		
P_{28}	1	3	4	6	10	21			
P_{29}	1	3	4	6	10	22	24	25	26
P_{30}	1	3	4	6	28	8			
P_{31}	1	3	4	6	28	27	25	26	
P_{32}	1	3	4	6	28	27	29	30	
P_{33}	1	3	4	6	28	27	30		
P_{34}	1	3	4	12	16	17			

Consider path P_{33} as shown in Table 4.2, which starts at bus 1 and terminates at bus 30. The intermediate buses are 3, 4, 6, 28 and 27. The lines that constitute the path are L_2, L_4, L_7, L_{41}, L_{36} and L_{38}. Thus the set ζ is {L_2, L_4, L_7, L_{41}, L_{36} and L_{38}}. The PVSI of the path can be calculated as

$$PVSI_{P33} = (LVSI_{L2,\,3} \times LVSI_{L4,\,4} \times LVSI_{L7,\,6} \times LVSI_{L41,\,28} \times LVSI_{L36,\,27} \times LVSI_{L38,\,30})$$
$$= (0.9086 \times 0.9822 \times 0.9975 \times 0.9973 \times 0.9603 \times 0.9378)$$
$$= 0.7995$$

Table 4.3 *PVSI* values of all the power flow paths given in Table 4.2

Path no	*PVSI*	Path no	*PVSI*
P_1	0.8802	P_{18}	0.8537
P_2	0.8925	P_{19}	0.8653
P_3	0.8814	P_{20}	0.8884
P_4	0.8644	P_{21}	0.8136
P_5	0.8576	P_{22}	0.8021
P_6	0.8694	P_{23}	0.8012
P_7	0.8694	P_{24}	0.8742
P_8	0.8516	P_{25}	0.8865
P_9	0.8177	P_{26}	0.8754
P_{10}	0.8925	P_{27}	0.8518
P_{11}	0.8174	P_{28}	0.8635
P_{12}	0.8059	P_{29}	0.8121
P_{13}	0.8049	P_{30}	0.8865
P_{14}	0.8124	P_{31}	0.8119
P_{15}	0.8641	P_{32}	0.8004
P_{16}	0.8761	P_{33}	**0.7995**
P_{17}	0.8773	P_{34}	0.8069

The *PVSI* of all power flow paths is then evaluated through equation (4.18), as explained in the above example, and the results found are given in Table 4.3. Similarly, the *PVSI* of other power flow paths originating at different source buses can also be evaluated. In this study, the power flow path that has the lowest value of

PVSI is considered as the most heavily loaded path or critical path that is vulnerable to voltage collapse. The value of *PVSI* of the most heavily loaded path is considered as the overall voltage stability index of the system. Therefore the voltage stability index (*VSI*) of the power system is expressed as follows

$$VSI = \min(PVSI_m) \tag{4.19}$$

where m varies from 1 to n and 'n' is total number of possible power flow paths originating from all source buses (Slack and *PV* buses)

Out of all the possible power flow paths; path P_{33} (given in Table 4.2) has the minimum *PVSI* (0.7995). Hence the critical path at base load condition is the path P_{33} (1-3-4-6-28-27-30). The last bus of the critical power flow path is considered as the weakest or critical bus in the system. The branch in the critical power flow path that has the highest value of *LL* is considered as the most heavily loaded branch. At base load condition, bus 30 is identified as the critical bus because it is the last bus of the critical power flow path (P_{33}). The values of *LL* of all lines in the identified critical power flow path (P_{33}) are given Table 4.4 and which indicates that line L_2 connected between bus 1 and bus 3 has the highest value of '*LL*' (0.1466). Hence line L_2 is identified as the critical line. However, as the load level changes, power flow paths may also change based on the *LVSI* of the lines at that load level. Thus, both critical bus and critical line may depend on the load level at which they are identified.

Table 4.4 *LL* values of all the lines in the identified critical power flow path

Line k	$LVSI_{ki}$	$LVSI_{kj}$	LL_k
L_2	1.0552	0.90859	**0.1466**
L_4	1.0162	0.98224	0.0339
L_7	1.0058	0.9913	0.0145
L_{41}	1.0025	0.99725	0.0052
L_{36}	1.0313	0.96029	0.0710
L_{38}	1.0614	0.9378	0.1236

4.3 Results and Discussions

The proposed method of determining the *VSI* is tested on the IEEE 30 bus system [53-54]. The *VSI* is determined for various load levels and the complex bus voltages needed for this purpose are obtained from load flow solutions. Load flow problem of the system is solved by uniformly increasing the load of all the buses with an increment of 1% of the base load, until the load flow algorithm gets diverged. It is assumed that the divergence of load flow algorithm at higher load levels is due to the occurrence of voltage collapse. The base load of the system is 310.23 MVA and the load flow algorithm successfully converged up to a load-multiplying factor (λ) of 1.57. Thus the critical load of the system is considered as 310.23 x 1.57 = 487.061 MVA. Beyond the load multiplying factor of 1.24, all *PV* buses reached their reactive power limits and became *PQ* buses, so only slack bus is available as reactive power source. When the load of the system is increased from base load to critical load, the critical power flow path identified remains the same as based load (i.e. 1-3-4-6-28-27-30). Throughout the load increase, it is observed that the line (L_2) between buses 1 and 3 is the critical line or heavily loaded line as '*LL*' of the line has the highest value. It is also observed that the bus 30 is the last bus in the critical power flow path. However, in other systems critical line and critical bus may change as the load level is changed.

The variation of *VSI* against the load-multiplying factor (λ) is shown in Fig. 4.9. It can be seen in Fig. 4.9 that the relationship between *VSI* and λ is nonlinear and it decreases monotonically with load. In power system planning, the maximum loading point can be determined by successively increasing the load and checking the existence of solution through load flow program. But in power system operation, sometimes it may be necessary to estimate the system maximum loading point without practically generating the entire *VSI* characteristic. For such a case, an extrapolation technique is to be used. Because of nonlinear characteristic of *VSI*, a linear extrapolation technique may provide erroneous results. However, by making the characteristic more or less linear, a better estimation of critical load can be found.

It can be noticed in Fig. 4.9 that the variation of *VSI* against λ is more or less parabolic. For such a characteristic one can easily be recognized that VSI^2 *vs* λ will have less non-linearity.

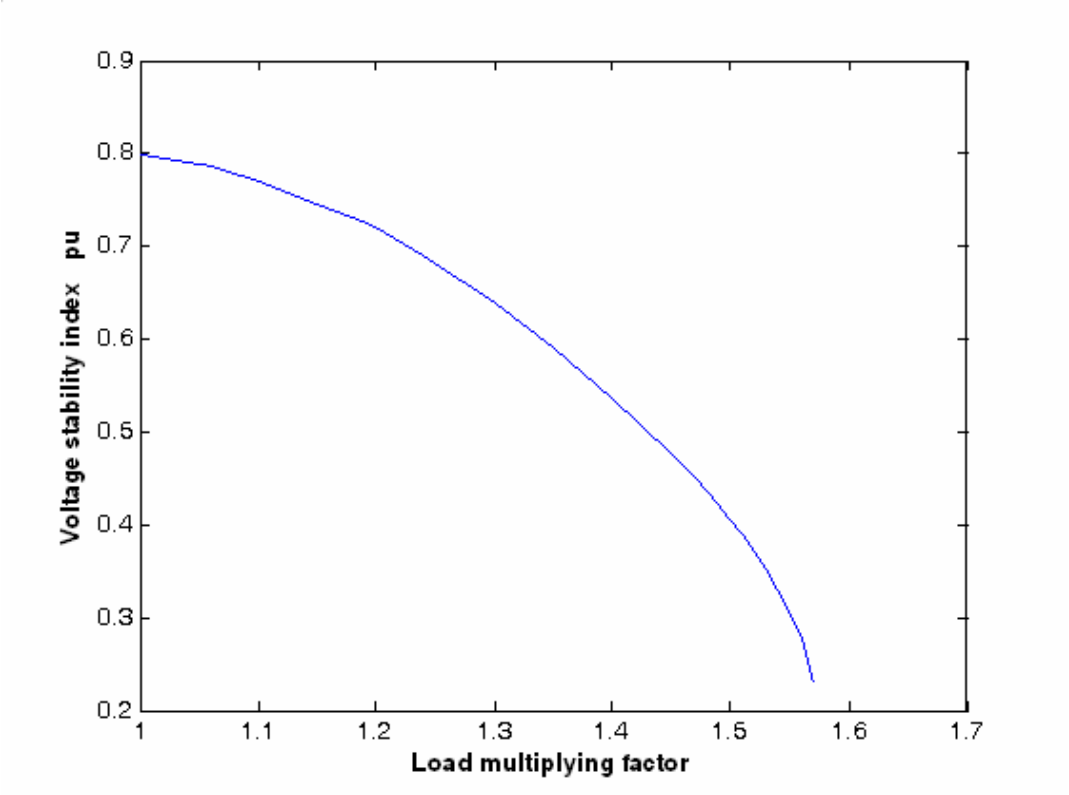

Fig. 4.9 Variation of the *VSI* for with load multiplying factor

The value of critical load multiplier factor (λ_{cr}) found by linear extrapolation of *VSI* (using the present and immediate past operating points) is given in Table 4.5. The Newton-Raphson load flow method projects λ_{cr} as 1.57. From Table 4.5 it can be seen that the error in the estimated critical load is very high. The values of critical load multiplier factor estimated by linear extrapolation of VSI^2 - λ characteristic (curve b in Fig. 4.10) are given in Table 4.6. The errors in the estimated values are also given in Table 4.6. Results of Tables 4.6 clearly indicate that the error is significantly reduced and in fact for λ greater than 1.3, the maximum error observed is around 5%.

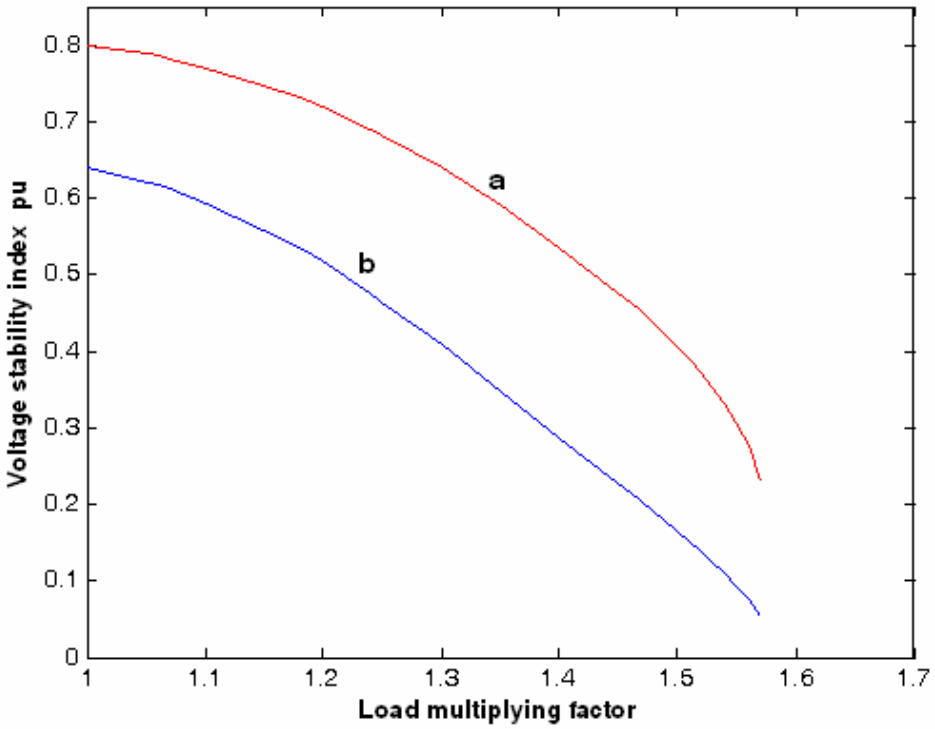

Fig. 4.10 Variation of *VSI* (curve a) and VSI^2 (curve b) with load multiplying factor

Table 4.5 *VSI*, estimated critical load multiplying factor (λ_{cr}) and % error

λ	*VSI*	Estimated λ_{cr}	%Error
1	0.7995	3.64	132.29
1.1	0.7693		
1.2	0.7204	2.67	70.26
1.3	0.6388	2.08	32.66
1.4	0.5364	1.92	22.54
1.5	0.4057	1.81	15.31
1.57	0.2303	1.73	10.27

Table 4.6 VSI^2, estimated critical load multiplying factor λ_{cr} and % error

λ	VSI^2	Estimated λ_{cr}	%Error
1	0.6392	2.35	49.68
1.1	0.5919		
1.2	0.5189	1.91	21.60
1.3	0.4081	1.66	5.70
1.4	0.2877	1.63	3.82
1.5	0.1646	1.63	3.82
1.57	0.0531	1.64	4.46

Identification of optimal location for installing series/shunt reactive compensations is critical for any power system. In this study, L_2 is identified as the most heavily loaded line. The loading of the line (and hence *LL*) can be reduced by installing a series capacitor. For verification purpose, a series capacitor is placed in different lines around the identified critical line (L_2). The critical load multiplying factor (λ_{cr}) of the system is then determined from the load flow solutions with a fixed series capacitive reactance of 0.1 pu in lines between buses 1&3, 2&4, 2&5, and 2&6 i.e. lines L_2, L_3, L_5 and L_6 and the results found are given in Table 4.7. From Table 4.7, it can be observed that the series capacitive reactance in line L_2 provide the highest value of λ_{cr} and the corresponding critical load is (1.67*310.23) 518.08 MVA. Hence from the results (Table 4.7) it can be concluded that the technique presented in the thesis correctly identified the weakest line of the system.

Similarly, a 0.5 pu of fixed shunt capacitive support is placed at different buses around the identified critical bus (bus 30). The value of λ_{cr} obtained with the fixed capacitor support at load buses 5, 7, 26 and 30 are given in Table 4.8. From Table 4.8

it can be observed that the support at bus 30 could provide the highest value of λ_{cr} and hence it can be concluded that bus 30 indeed the weakest bus in the system.

Table 4.7 Critical load multiplying factor with series capacitive reactance

Series capacitor location	From bus - To bus	λ_{cr}
No capacitor	-	1.57
Line L_2	1-3	1.67
Line L_3	2-4	1.59
Line L_5	2-5	1.64
Line L_6	2-6	1.61

Table 4.8 Critical load multiplying factor with shunt capacitive reactance

Shunt capacitor location	λ_{cr}
No Capacitor	1.57
Bus 5	1.65
Bus 7	1.66
Bus 26	1.65
Bus 30	1.67

4.4 Summary

In this chapter, initially an expression for line voltage stability index (*LVSI*) of a simple two-bus system is derived. The *LVSI* requires only the complex bus voltages and it does not need the generator, load and line parameters. Therefore, for a general power system, *LVSI* of all lines can be determined using the complex bus voltages generated by the load flow program. Based on the *LVSI* values of lines, possible power flow paths are identified. This is followed by determining a voltage stability index of each power flow path (*PVSI*). The power flow path with minimum *PVSI* is assumed as the critical power flow path of the system. The *PVSI* of the critical path is

considered as the overall *VSI* of the system. Using the values of *VSI* at the present and past operating points, the critical load of the system is estimated. In addition, the critical line is identified based on *LVSI* values of all lines in the critical power flow path. The correctness of the identified critical line and critical bus is then verified by installing fixed capacitive support around the critical line and critical bus and finding the actual critical load multiplier factor through load flow solutions.

Chapter 5

Conclusions and Recommendations

5.1 Conclusions

In this study, the models of various power system components, such as on load tap changer (OLTC), over excitation limiter (OXL), automatic voltage regulator (AVR), generators, induction motors, etc. are first studied and then implemented using SIMULINK and MATLAB software. These models are then integrated to investigate the short-term and long-term voltage stability of simple power systems.

The phenomenon of short-term voltage stability of a simple power system caused by a heavily loaded induction motor load is presented in this study following a large disturbance, the short-term stability is investigated by using the network *P-V* curve and the motor *P-V* curve generated at an internal point of the motor. The results obtained by using the above *P-V* curves are then verified through observing the system states in time domain generated by SIMULINK and MATLAB software. The above results are able to demonstrate the mechanism of short-term voltage collapse following a sudden large disturbance. For a 3-phase fault at the terminals, both the voltage and power of the motor become zero and remains same during the faulted period and that cause to decelerate the motor. However, once the fault is cleared, motor terminal voltage and power suddenly increase. Depending on fault clearing time, the motor may or may not reach an acceptable stable operating point in post fault period. A technique of determining the critical fault clearing time (t_{cr}) that guarantees stable post fault operation of the motor is also presented. Simulation results indicated that the motor slip initially increases slightly and then decreases to a stable value, if the fault is cleared within t_{cr}. However, when the fault is cleared after t_{cr}, slip increases monotonically and ultimately the motor stalls. It is also observed from the results that the value of t_{cr} increases when a shunt capacitor is installed at the motor terminal.

The phenomenon of long-term voltage stability of a power system is investigated by considering the dynamics of both fast and slow-acting devices. In general, the fast-acting devices reached the quasi steady-state equilibrium point before the start of operation of the slow-acting devices such as OLTC of the transformer, OXL of a generator, etc., A computer program is developed in MATLB and SIMULINK environment to investigate the long-term voltage stability of a simple power system.

The simulation results obtained by considering the dynamics of all devices are systematically described. It was observed that, following a disturbance, the generator field current may exceed the limit in order to restore the desired terminal voltage. However, excessive field current for a prolonged period may activate the OXL to prevent overheating of the generator field windings. Activation of OXL decreases the field current and hence the generator terminal voltage and that might initiate the voltage collapse. However, supplying adequate reactive power from other sources can prevent the voltage collapse process.

A technique of determining the static voltage stability index (*VSI*) of a power system is also presented. First an expression of line voltage stability index (*LVSI*) is derived for a simple two bus system. The concept is then extended for a general power system. Based on the *LVSI* values, a number of possible power flow paths originating at source buses are identified. The voltage stability index (*VSI*) of each power flow path is then determined. The path that has the minimum *VSI* is considered as the critical or heavily loaded path. The *VSI* of the critical path is then used to estimate the system critical load at the voltage collapse point by using linear extrapolation. The results obtained are then compared with the corresponding actual values obtained by repetitive load flow simulations. It was observed that the error in the estimated value is very high especially at lower load levels. However, the error can significantly be reduced by using the squared value of *VSI* instead of *VSI*. The weakest bus and heavily loaded line of the system are also identified. The voltage stability limit of the system is then improved by placing shunt capacitor at the weakest bus and series capacitor in the heavily loaded line. The correctness of the identified weakest bus and heavily loaded line is also verified by placing series and shunt capacitors at various locations and comparing the corresponding critical loads obtained by load flow simulations.

5.2 Recommendations

In this study, the short-term and long-term voltage stability of a simple power system is investigated. The equations derived and SIMULINK and MATLAB program developed are not very general but specific to the study systems used in this investigation. So, it is worthwhile to extend the concept further for a general power

system. In this study, the voltage stability problem is alleviated using fixed capacitor compensation. However, the dynamics of the system may further be improved by using variable reactive compensation instead of fixed compensation. The possibility of using variable reactive compensation, such as static var compensators (*SVC*), voltage-source converter based compensation etc., to alleviate the voltage stability problem can be investigated.

The system critical load estimated by using the static voltage stability index derived in this study provides erroneous results. This happened because of non-linear characteristic of the index. By a trial and error approach, it was found that the error can significantly be reduced by using the squared value of voltage stability index. However, a more accurate estimation of critical load can be obtained by deriving a more linear voltage stability index. Further investigation with the mathematical justification to derive such an index would be very useful.

Author's Publications

[1] M. H. Haque and U. M. R. Pothula, "Evaluation of dynamic voltage stability of a power system," *IEEE Power technology conference (POWERCON)*, Singapore, 20-24, Nov 2004.

[2] U. M. R. Pothula and M. H. Haque, "Effect of Induction motor load on short term voltage stability," *National Power Systems Conference* (NPSC-2004), Indian Institute of Technology, Madras, Chennai, India, 27-30 Dec 2004.

Bibliography

[1] C. W. Taylor, "Power system voltage stability", New York: *McGraw-Hill*, 1994.

[2] P. Kundur, "Power system stability and control", New York: *McGraw-Hill*, 1994.

[3] T. V. Cutsem and C. Vournas, "Voltage stability of electric power system", Norwell, MA: *Kluwer*, 1998.

[4] V. Ajjarapu and B. Lee, "Bibliography on voltage stability", *IEEE Transaction on Power Systems*, Vol. 13, No. 1, pp. 115-125, 1998.

[5] T. V. Cutsem, "Voltage instability: phenomena, countermeasures, and analysis methods", *Proceedings of the IEEE*, Vol. 88, No. 2, pp. 208-226, February 2000.

[6] D. Novosel, M. M. Begovic and V. Madani, "Shedding light on blackouts", *IEEE Power and Energy Magazine*, Vol. 2, No.1, pp. 32-43, Jan/Feb 2004.

[7] J. Bialek, "Are blackouts contagious?", *IEE Power Engineer,* pp. 10-13, Dec/Jan, 2003/04.

[8] B. M. Weedy and B. R. Cox, "Voltage stability of radial power links", *Proc. Inst. Elect. Eng*., Vol. 115, pp. 528-536, 1968.

[9] V. A. Venikov, V. A. Stroev, V. I. Idelchick, and V. I. Tarasov, "Estimation of electrical power system steady-state stability", *IEEE Transaction on Power Apparatus and Systems,* Vol. 94, pp. 1034-1040, 1975.

[10] IEEE/PES Power system stability subcommittee special publication, "Voltage stability assessment, procedures and guides", 2001.

[11] C. D. Vournas, E. G. Potamianakis, C. Moors and T. V. Cutsem, "An educational simulation tool for power system control and stability", *IEEE Transaction on Power Systems*, Vol. 19, No. 1, pp. 48-55, 2004.

[12] F. Gubina and B. Strmcnik, "Voltage collapse proximity index determination using voltage phasors approach", *IEEE Transaction on Power Systems*, Vol. 10, No.2, pp. 788-792, May 1995.

[13] IEEE/CIGRE Joint task force report on, "Definition and classification of power system stability", *IEEE Transaction on Power Systems*, Vol. 19, pp. 1387-1401, 2004.

[14] CIGRE WG 38.02 Task force No.10, "Modeling of voltage collapse including dynamic phenomena", Technical report of task force 38.02.10, draft 3, CIGRE, June 1992.

[15] H. Ohtsuki, A. Yokoyama and Y. Sekine, "Reverse action of on load tap changer in association with voltage collapse", *IEEE Transaction on Power Systems*, Vol. 6, No. 1, pp. 300-306, 1991.

[16] T. X. Zhu, S .K. Tso and K. L. Lo, "An investigation into the OLTC effects on voltage collapse", *IEEE Transaction on Power Systems*, Vol. 15, pp. 515-521, 2000.

[17] M. Z. El-Sadak et al, "Combined use of tap-changing transformer and static VAR compensator for enhancement of steady–state voltage stabilities", *Electric Power Systems Research (EPSR*), pp. 47-55, 1998.

[18] D. Thukaram, L. Jenkis, H. P. Kincha, G. Yesuratnam and B. R. Kumar, "Monitoring the effects of on load tap changing transformers on voltage stability", *Proc IEEE Conference (POWERCON)*, 2004.

[19] K. Walve, "Modeling of power system components at severe disturbances", *in Int. Conf. Large High Voltage Electric Systems,* Paris, France, Aug. 27- Sept. 4, 1986.

[20] S. Repo, "Online voltage stability assessment of powers system- an approach of black-box modeling", Publication 344, Tampere University of Technology, Tampere, 2001.

[21] I. Dobson and L. Lu, "Voltage collapse precipitated by the immediate change in stability when generator reactive power limits are encountered", *IEEE Transactions on circuits and systems-I*, Vol. 39, No. 9, pp. 762-766, 1992.

[22] M. L. Crow and J. Ayyagari, "The Effect of Excitation limits on voltage stability", *IEEE Transactions on Circuits and Systems-I*, Vol. 42, No. 12, pp. 1022-1026, 1995.

[23] C. D. Vournas, G. A. Manos, P.W. Sauer and M. A. Pai, "Effect of over excitation limiters on power system long term modeling", *IEEE Transaction on Energy Conversion*, Vol. 14, No. 4, pp. 1529-1536, 1999.

[24] D. J. Hill, "Nonlinear dynamic load models with recovery for voltage stability studies", *IEEE Transaction on Power Systems*, Vol. 8, pp. 166-176, 1993.

[25] IEEE task force report on, "Standard load models for power flow and dynamic performance simulation", *IEEE Transaction on Power Systems*, Vol. 10, No. 3, pp. 1302-1313, August 1995.

[26] IEEE task force report on, "Load representation for dynamic performance analysis", *IEEE Transaction on Power Systems*, Vol. 8, No. 2, pp. 472-482, 1992.

[27] G. D. Prasad and M. A. Al-Mulhim, "Performance evaluation of dynamic load models for voltage stability analysis", *Electrical Power & Energy Systems*, Vol. 19, No. 8, pp. 533-540, 1997.

[28] R. Balanathan, N. C. Pahalawaththa, U. D. Annakkage, "Modeling induction motor loads for voltage stability Analysis", *Electrical Power & Energy Systems,* Vol. 24, pp. 469-480, 2002.

[29] J. A. Diaz de Leon II and C. W. Taylor, "Understanding and solving short-term voltage stability problems", *IEEE PES Summer Meeting*, pp. 745-752, 2002.

[30] Y. Sekine and H. Ohtsuki, "Cascaded voltage collapse", *IEEE Transaction on Power Systems*, Vol. 5, No. 1, pp. 250-256, February 1990.

[31] M. H. Haque, "Determination of steady state voltage stability limit with shunt FACTS devices", *Proc. V International Power Engineering Conference (IPEC 2001*), 17-19 May, Singapore, pp. 564-569, 2001.

[32] M. Chebbo, M. R. Irving and M. J. H. Sterling, "Voltage collapse proximity indicator: behaviour and implications", *IEE Proceedings-C,* Vol. 139, pp. 241-252, 1992.

[33] R. A. Schlueter, I. Hu, M. W. Chang, J. C. Lo and A. Costi, "Methods for determining proximity to voltage collapse", *IEEE Transaction on Power Systems*, Vol. 6, No. 1, pp. 285-292, 1991.

[34] C. A. Canizares and F. L. Alvarado, "Point of collapse and continuation methods for large AC/DC systems", *IEEE Transaction on Power Systems*, Vol. 8, No. 1, 1993.

[35] T. T. Lie, "Method of identifying the strategic placement for compensation devices", *IEEE Transaction on Power Systems*, Vol. 10, No. 3, pp. 1448-1453, 1995.

[36] C. A. Canizares, A. C. Z. de Souza, and V. H. Quintana, "Comparison of performance indices for detection of proximity to voltage collapse", *IEEE Transaction on Power Systems*, Vol. 11, pp. 1441-1450, August 1996.

[37] P. A. Lof, G. Andersson and D. H. Hill, "Voltage stability indices for stressed power systems", *IEEE Transaction on Power Systems*, Vol. 8, pp. 326-335, 1993.

[38] N. Flatabo, R. Ognedal and T. Carlsen, "Voltage stability condition in a power transmission system calculated by sensitivity methods", *IEEE Transaction on Power Systems,* Vol. 5, No. 4, pp. 1286-1293, 1990.

[39] K. Vu, M. G. Begovic, D. Novosel and M. M. Saha, "Use of local measurements to estimate voltage-stability margin", *IEEE Transaction on Power Systems,* Vol. 14, No. 3, pp. 1029-1035, 1999.

[40] M. H. Haque, "On-line monitoring of maximum permissible loading of a power system within voltage stability limits", *Generation, Transmission and Distribution, IEE Proceedings-*, Volume: 150, pp. 107-112, 2003.

[41] B. H. Chowdary and C. W. Taylor "Voltage stability analysis: V-Q power flow simulation versus dynamic simulation", *IEEE Transaction on Power Systems*, Vol. 15, No. 4, pp. 1354-1359, 2000.

[42] M. H. Haque, "Use of V-I characteristic as a tool to assess the static voltage stability limit of a power system", *Generation, Transmission and Distribution, IEE Proceedings*, Vol. 151 pp. 1-7, 2004.

[43] A. Mohamed and G. B. Jasmon, "Determining the weak segment of power system with voltage stability considerations", *Elect. Mach. Power Systems*, vol. 24, pp. 555-568, 1996.

[44] H. Lee, and K. Y. Lee, "Dynamic and static voltage stability enhancement of power systems", *IEEE Transaction on Power Systems*, Vol. 8, No. 1, pp. 231-238, 1993.

[45] P. Kessel and H. Glavitsch, "Estimating the voltage stability of a power system," *IEEE transaction on power delivery*, Vol. PWRD-1, pp. 346-354, 1986.

[46] R. Khatib, R. F. Nuqui, M. R. Ingram and A. G. Phadke, "Real- time estimation of security from voltage collapse using synchronized phasor measurements", *Proc. of IEEE Power Engineering Society General Meeting*, pp. 582- 588, 2004.

[47] C. Rehtanz and J. Bertsch**,** "Wide area measurement and protection system for emergency voltage stability control", *Proc. IEEE PES Winter Meeting*, January 2002.

[48] D. Karlsson, M. Hemmingsson and S. Lindal**,** "Wide area system monitoring and control", *IEEE Power and Energy Magazine*, Vol. 2, No. 5, pp. 68-76, Sep/Oct 2004.

[49] M. H. Haque, "Determination of steady state voltage stability limit using *P-Q* curve", *IEEE Power Engineering Review*, pp. 71-72, April 2002.

[50] R. K. Gupta, Z. A. Alaywan, R. B. Stuart and T. A. Reece**,** "Steady state voltage instability operations perspective", *IEEE Transaction on Power Systems*, Vol. 5, No. 4, pp. 1345-1354, 1990.

[51] W. D. Stevenson, "Elements of power system analysis", *McGraw-Hill International*, 1982.

[52] G. W. Stagg and A. H. El-Abiad, "Computer methods in power system analysis", *McGraw-Hill International*, 1981.

[53] Power Systems Test Case Archive; http://www.ee.washington.edu/research/pstca/

[54] H. Saadat, "Power system analysis", *McGraw-Hill*, Singapore, 1999.

Appendix A

Test System Data for Dynamic Voltage Stability

System Reactance in pu (on 800MVA base)

Incase of Fig. 3.1 (Short-Term)

V_{th} = 1.05, X_{th} = 0.08, X_{14} = 0.128 (double line), X_{14} = 0.256, X_C=0.1875

Incase of Fig. 3.10 (Long-Term)

V_{th} = 1.08, X_{th} = 0.08, X_{14} = 0.2216 (double line), X_{24} = 0.128, X_{34} = 0.032.

Incase of Critical Fault Clearing Time

V_{th} = 1.05, X_{th} = 0.08, X_{14} = 0.2216 (double line), X_{24} = 0.128, X_{34} = 0.032.
X_C=0.3125

Synchronous Generator data in pu (on 800MVA base)

X_d = 3.36, X_q = 3.36, X'_d = 0.64, T'_{do}= 8 s, $\omega_0 = 2\pi 50$ rad/s, H = 3.5 s, D = 0.164 pu.

AVR Parameters

G = 50, T = 0.1 s, $v_{fd}^{\min} = 0$ pu, $v_{fd}^{\max}$ =5.0 pu.

OXL Parameters

$I_{fd}^{\min}$ = 2.825 pu, S_1 = 1, S_2 = 2, K_1 = 20, K_2 = 0.1, K_r = 1, K_i = 0.1.

OLTC Data

$r^{\min} = 0.9$, $r^{\max} = +1.1$, $\Delta r = 0.0625$, V_{ref} = 1.0 pu, d = 0.015, T_d = 20 s, T_m = 10 s.

Induction Motor in pu (on 800MVA base)

R_s = 0,X_s = 0.1, X_m = 3.2, R_r = 0.018; X_r = 0.18, t_m = 0.8 pu.

H = 0.5s for critical fault clearance time determination, H = 2.5 for short-term case.

Exponential Load

Q_0/P_0 = 0.5, α = 2.0, β = 2.0, V_0 = 1.0.

IEEE 30 Bus Test System Data for Static Voltage Stability Index Determination

Bus data

Bus no	Bus Code*	Voltage Magnitude	Angle	Load		Generator		Q_{min}	Q_{max}	Static
				MW	MVAR	MW	MVAR			MVAR
1	1	1.06	0	0	0	0	0	0	0	0
2	2	1.043	0	21.7	12.7	40	0	-40	50	0
3	0	1	0	2.4	1.2	0	0	0	0	0
4	0	1.06	0	7.6	1.6	0	0	0	0	0
5	2	1.01	0	94.2	19	0	0	-40	40	0
6	0	1	0	0	0	0	0	0	0	0
7	0	1	0	22.8	10.9	0	0	0	0	0
8	2	1.01	0	30	30	0	0	-10	40	0
9	0	1	0	0	0	0	0	0	0	0
10	0	1	0	5.8	2	0	0	0	0	19
11	2	1.082	0	0	0	0	0	-6	24	0
12	0	1	0	11.2	7.5	0	0	0	0	0
13	2	1.071	0	0	0	0	0	-6	24	0
14	0	1	0	6.2	1.6	0	0	0	0	0
15	0	1	0	8.2	2.5	0	0	0	0	0
16	0	1	0	3.5	1.8	0	0	0	0	0
17	0	1	0	9	5.8	0	0	0	0	0
18	0	1	0	3.2	0.9	0	0	0	0	0
19	0	1	0	9.5	3.4	0	0	0	0	0
20	0	1	0	2.2	0.7	0	0	0	0	0
21	0	1	0	17.5	11.2	0	0	0	0	0
22	0	1	0	0	0	0	0	0	0	0
23	0	1	0	3.2	1.6	0	0	0	0	0
24	0	1	0	8.7	6.7	0	0	0	0	4.3
25	0	1	0	0	0	0	0	0	0	0
26	0	1	0	3.5	2.3	0	0	0	0	0
27	0	1	0	0	0	0	0	0	0	0
28	0	1	0	0	0	0	0	0	0	0
29	0	1	0	2.4	0.9	0	0	0	0	0
30	0	1	0	10.6	1.9	0	0	0	0	0

* Bus code: 0 for PQ bus, 1 for Slack bus and 2 for PV bus

Line data

Bus from	Bus to	R pu	X pu	1/2B pu	t_r	Line no
1	2	0.0192	0.0575	0.0264	1	1
1	3	0.0452	0.1852	0.0204	1	2
2	4	0.057	0.1737	0.0184	1	3
3	4	0.0132	0.0379	0.0042	1	4
2	5	0.0472	0.1983	0.0209	1	5
2	6	0.0581	0.1763	0.0187	1	6
4	6	0.0119	0.0414	0.0045	1	7
5	7	0.046	0.116	0.0102	1	8
6	7	0.0267	0.082	0.0085	1	9
6	8	0.012	0.042	0.0045	1	10
6	9	0	0.208	0	0.978	11
6	10	0	0.556	0	0.969	12
9	11	0	0.208	0	1	13
9	10	0	0.11	0	1	14
4	12	0	0.256	0	0.932	15
12	13	0	0.14	0	1	16
12	14	0.1231	0.2559	0	1	17
12	15	0.0662	0.1304	0	1	18
12	16	0.0945	0.1987	0	1	19
14	15	0.221	0.1997	0	1	20
16	17	0.0824	0.1923	0	1	21
15	18	0.1073	0.2185	0	1	22
18	19	0.0639	0.1292	0	1	23
19	20	0.034	0.068	0	1	24
10	20	0.0936	0.209	0	1	25
10	17	0.0324	0.0845	0	1	26
10	21	0.0348	0.0749	0	1	27
10	22	0.0727	0.1499	0	1	28
21	22	0.0116	0.0236	0	1	29
15	23	0.1	0.202	0	1	30
22	24	0.115	0.179	0	1	31
23	24	0.132	0.27	0	1	32
24	25	0.1885	0.3292	0	1	33
25	26	0.2544	0.38	0	1	34
25	27	0.1093	0.2087	0	1	35
28	27	0	0.396	0	0.968	36
27	29	0.2198	0.4153	0	1	37
27	30	0.3202	0.6027	0	1	38
29	30	0.2399	0.4533	0	1	39
8	28	0.0636	0.2	0.0214	1	40
6	28	0.0169	0.0599	0.065	1	41